Thesis for the Degree of Master of Engineering

Solar energy-assisted lithium-ion battery using photoelectrochromic property

Taeheui Kim

Department of Chemical Engineering
The Graduate School
Pukyong National University

February 2021

Solar energy-assisted lithium-ion battery using photoelectrochromic property

(광전기변색 특성을 응용한 광감응 리튬 이온 전지)

Advisor: Dr. Yiseul Park

by

Taeheui Kim

A thesis submitted in partial fulfillment of the requirements for the degree of Master of Engineering

Department of Chemical Engineering, The Graduate School,

Pukyong National University

February 2021

김태희의 공학석사 학위논문을 인준함.

2021 년 2 월 19 일

위 원 장 공학박사 임 준 혁 (인)

위 원 공학박사 권 혁 택 (인)

위 원 공학박사 박 이 슬 (인)

Contents

List of figures

List of schemes

List of tables

광전기변색 특성을 응용한 광감응 리튬 이온 전지

김 태 희

부 경 대 학 교 대 학 원 화 학 융 합 공 학 부

요 약

본 연구에서는 태양광 에너지를 활용하여 소형 에너지 저장 장치의 전기화학적 특성을 개선하고자 광감응 리튬 이온 전지(solar energy-assisted lithium-ion battery)를 제시하였다. 광감응 리튬 이온 전지의 양극으로 광흡수 성질을 지닌 삼산화 텅스텐(WO_3) 전극을 사용하여 리튬화(lithiation)/탈리튬화(delithiation) 과정 중 빛에 따른 전기화학적 특성 변화를 측정 및 분석하였다. 또한, 태양광 조사가 리튬화/탈리튬화 과정에 미치는 영향을 파악하였다. WO_3 전극에 태양광을 조사하였을 때, 전지의 용량이 태양광을 조사하지 않았을 때보다 증가하였다. WO_3 가 태양광 조사에 의해 광전자를 생성하여 전극의 전기화학적 특성에 영향을 주기 때문으로 해석된다. 태양광 조사에 의해 생성된 광전자가 리튬 이온의 삽입(intercalation)에 사용되어 전지의 용량을 증가시킬 수 있을 뿐 아니라, 전극의 전자 수송을 촉진하여 용량이 향상되는 것으로 여겨진다. 빛의 효과는 지속적인 태양광 조사 시 극대화되고 간헐적인 태양광 조사에서도 전지의 용량은 유지되었다. 이는 태양광 조사에 의해 생성된 광전자가 축적된 결과로 해석된다. 리튬화/탈리튬화를 반복하여 진행하면 태양광을 조사하지 않았을 때 WO_3 는 상대적으로 큰 작동 전위로 인해 화학적 안정성에 영향을 미친다. 반면, 태양광을 조사하였을 때 WO_3 는 생성된 광전자로 인해 작은 작동 전위로 리튬화/탈리튬화가 일어나 전극의 안정성이 향상되었다.

I. Research background

1. Principle of lithium-ion battery

A battery is a device which directly converts the chemical energy of electrode material into electrical energy using an electrochemical reaction. Among various secondary rechargeable batteries, the lithium-ion battery is most widely studied and even commercialized due to the superior performance, enabled by high values of specific capacity, energy, power density, and high operating potential.[1-4]

As shown in scheme 1, the lithium-ion battery is composed of an anode, a cathode, an electrolyte, and a separator. The separator prevents electrical contact between the anode and cathode. The electrolyte is a medium that helps the movement of ions with properties of electrochemical stability and high thermal range. The anode stores and releases lithium ions, and the cathode is a source of lithium ions, which determines the capacity and the average voltage of a battery. Commonly, lithium-ion batteries use transition metal oxide as an anode and carbon as a cathode.[2,4] During an electrochemical redox reaction, ions move between the anode and cathode while

electrons transfer synchronously between two electrodes through a conducting wire, through which the charge/discharge occurs.

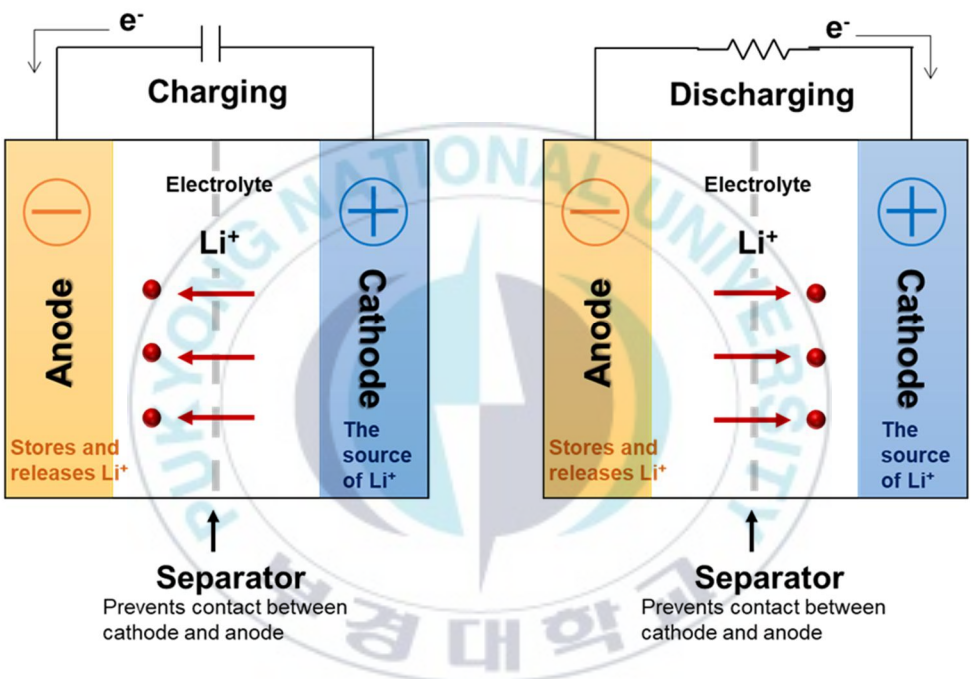

Scheme 1. Schematic illustration of the principle of a lithium-ion battery

2. Principle of a photocatalyst

Photocatalysts convert solar energy into chemical energy. When absorbing photons with energy above the gap between the valence band (VB) and the conduction band (CB), referred to as band-gap, the photocatalytic reaction can be initiated. When this reaction occurs, the electron-hole pair is formed, as shown in scheme 2. First, the electrons are excited from VB to CB, while the holes are generated in VB. And then, electron transfer is raised at the interface in detail. Photogenerated electrons in the CB can cause reduction reactions, and the photogenerated holes in the VB can cause oxidation reactions.[5,6]

Among various photocatalysts, semiconducting transition metals are attracting considerable interest due to their low cost and stable chemical stability.[7,8] Notably, WO_3 and its composite have been extensively used for photocatalysts.[9]

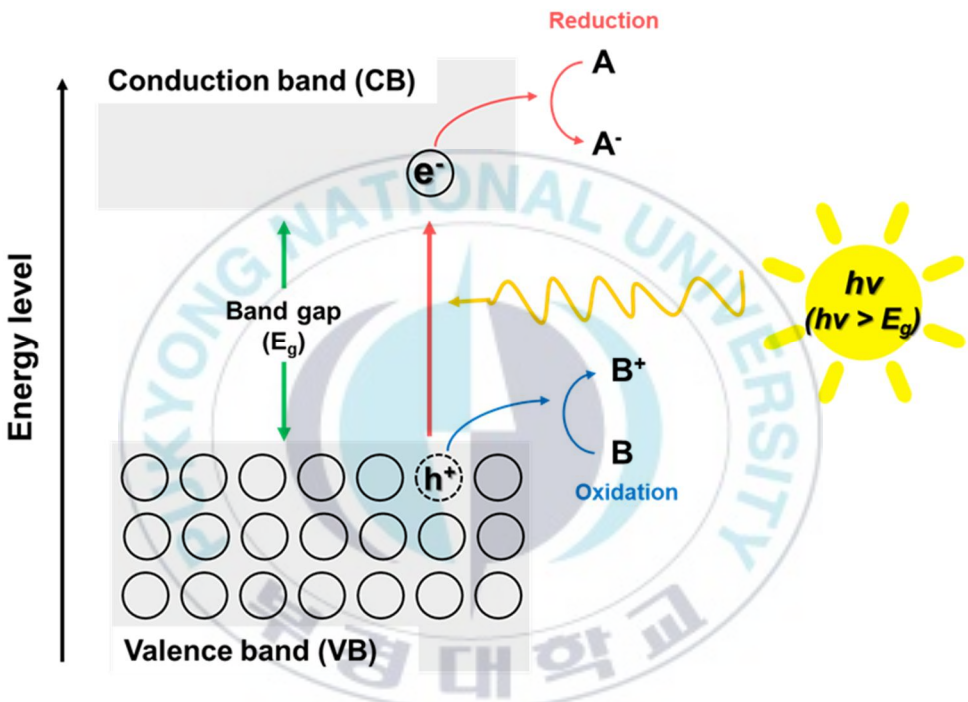

Scheme 2. Schematic illustration of the photocatalytic process on the semiconducting metal oxides.

3. Photoelectrochromism

Photoelectrochromism describes the reversible changes of color caused by faradaic reactions which are intercalation/extraction of small ions (ex. H^+, Li^+) by light irradiation.[7,10-12] In particular, WO_3 is widely used as one of the photoelectrochromic materials due to superior electron transport ability, high chemical stability, and sensitivity to visible light.[10,11,13,14] Among various phases of WO_3, the monoclinic phase is the most stable crystal phase and active photocatalyst.[7,15] Accordingly, we used monoclinic WO_3 in this study.

Ⅱ. Solar energy-assisted lithium-ion battery using photoelectrochromic property

1. Introduction

Recently, wearable devices in a variety of forms including watches, wrist bands, and eyewear are being extensively developed and commercialized due to the consumer's need to get information readily, anywhere. However, there is still a major technological hurdle that needs to be overcome: the battery problem. Accordingly, this is increasing the importance of developing energy storage devices, which are small, thin, and light.[16] Many researchers have attempted to fabricate energy storage systems using various active materials and substrates suitable for wearable devices. Among many, carbon-based fiber or paper substrates have been widely used.[16-18] However, these systems still have a limit on the volume capacity due to the use of a small amount of active material.

In order to overcome these limitations, we have tried to integrate solar energy into the energy storage system based on the fact that wearable devices are easily exposed to sunlight. In the case of a conventional solar-rechargeable battery, which is

combined with solar energy and battery system, a three-electrode system is being developed in which the conversion and storage of solar energy are performed at different electrodes[19-21], and so it inevitably becomes a large-scale system. Therefore, unlike the conventional solar-rechargeable battery concept, this study set out to improve the electrochemical property and performance by integrating solar energy into the conventional lithium-ion battery, which is composed of the two-electrode system. We refer to this concept and design as a "solar energy-assisted lithium-ion battery". The solar energy-assisted lithium-ion battery is composed of a photo-anode, which is light(photo)-sensitive material, and a cathode. Among the commercial lithium-ion battery electrode materials, tungsten oxide (WO_3), titanium dioxide (TiO_2), and iron (III) oxide (Fe_2O_3) have the light absorption property and widely used as photocatalysts in which photoelectrons are formed.[4,22-26] In particular, the WO_3 can be performed stable lithiation/delithiation due to photoelectrochromic property.[10,11] Therefore, in this study, we investigated the effect of light on electrochemical properties by preparing WO_3 as an anode and analyzed the working mechanism of the solar energy-assisted lithium-ion battery.

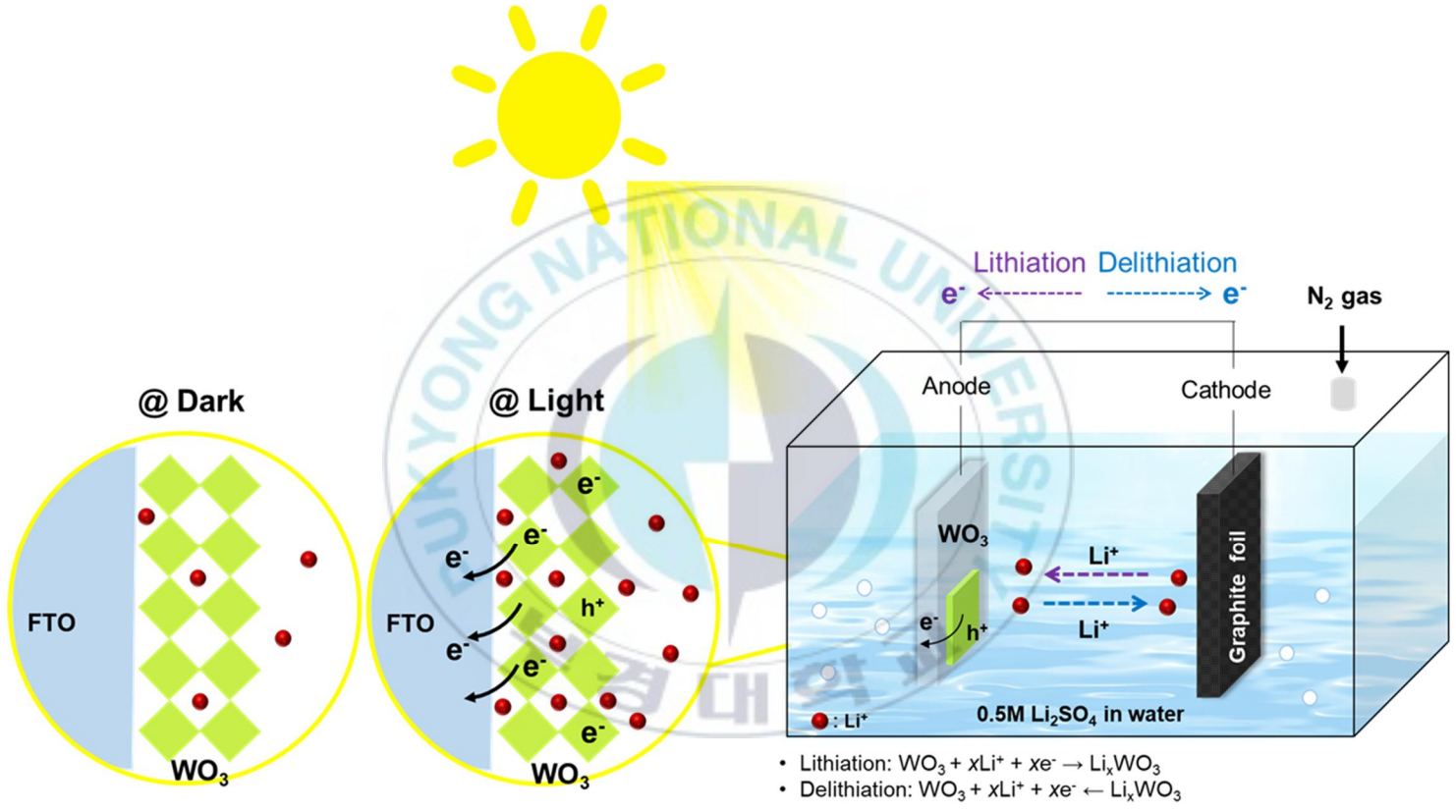

Scheme 3. Schematic illustration of the solar energy-assisted lithium-ion battery.

2. Experimental method

2.1. Electrode preparation

Tungsten trioxide (WO_3) thin films were prepared through an electrochemical deposition and doctor blade method coating on conducting fluorine doped tin oxide (FTO) glass substrate. The overall process of WO_3 electrode preparation is shown in scheme 4. Before the coating, the FTO glass was cleaned first with acetone and ethanol and then deionized water for 10minutes, respectively. And then, tungsten trioxide electrochemical deposition was conducted to improve adhesion for long-term performance by increasing roughness of FTO glass surface. The electrochemical deposition method was followed as reported previously.[27,28] **"**Tungsten powder (2.0grams, Sigma Aldrich) was dissolved in hydrogen peroxide solution (10ml, Junsei, 35% purity). After the exothermic reaction ended, 100ml of deionized water and 30ml of isopropyl alcohol (IPA) were added in the solution. A clean platinum (Pt) plate (5cm x 5cm) was immersed in the prepared solution for 15hours to eliminate excess residual hydrogen peroxide in the solution. The electrochemical deposition was carried out with three-electrode system, which included a working electrode (FTO glass, 1cm x 1 cm), a Pt wire as a counter electrode, and Ag/AgCl (with saturated KCl) as a reference electrode. A potential of

-0.4V (vs. Ag/AgCl) was applied to the working electrode for 15minutes. At the end of the deposition process, a potential of 0.2V (vs. Ag/AgCl) was applied on the working electrode for 5secondes to remove the blue coloration caused by the electron accumulation on WO_3 during the deposition process. The obtained WO_3 film was carefully washed with ethanol and deionized water, and then annealed in air at 450℃ for 1hour." After depositing WO_3 film, its slurry was mixed with tungsten trioxide powder (Sigma Aldrich) and Polyvinylidene fluoride powder (PVDF, Alfa) (8:1 by weight) in N-Methyl-2-pyrrolidone (NMP, Sigma Aldrich) using ball mill. The slurry was coated onto the WO_3 electrodeposited FTO by doctor-blade method. After coating, the electrode was dried under vacuum at 120℃ for 12hours.[29] Finally, the as-prepared WO_3 electrode was subjected to press for 30seconds to improve adhesion between substrate and WO_3 film.

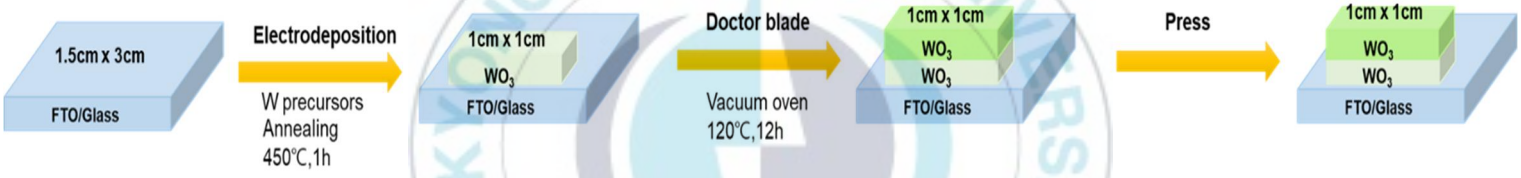

Scheme 4. Schematic illustration of the WO_3 thin film electrode preparation method

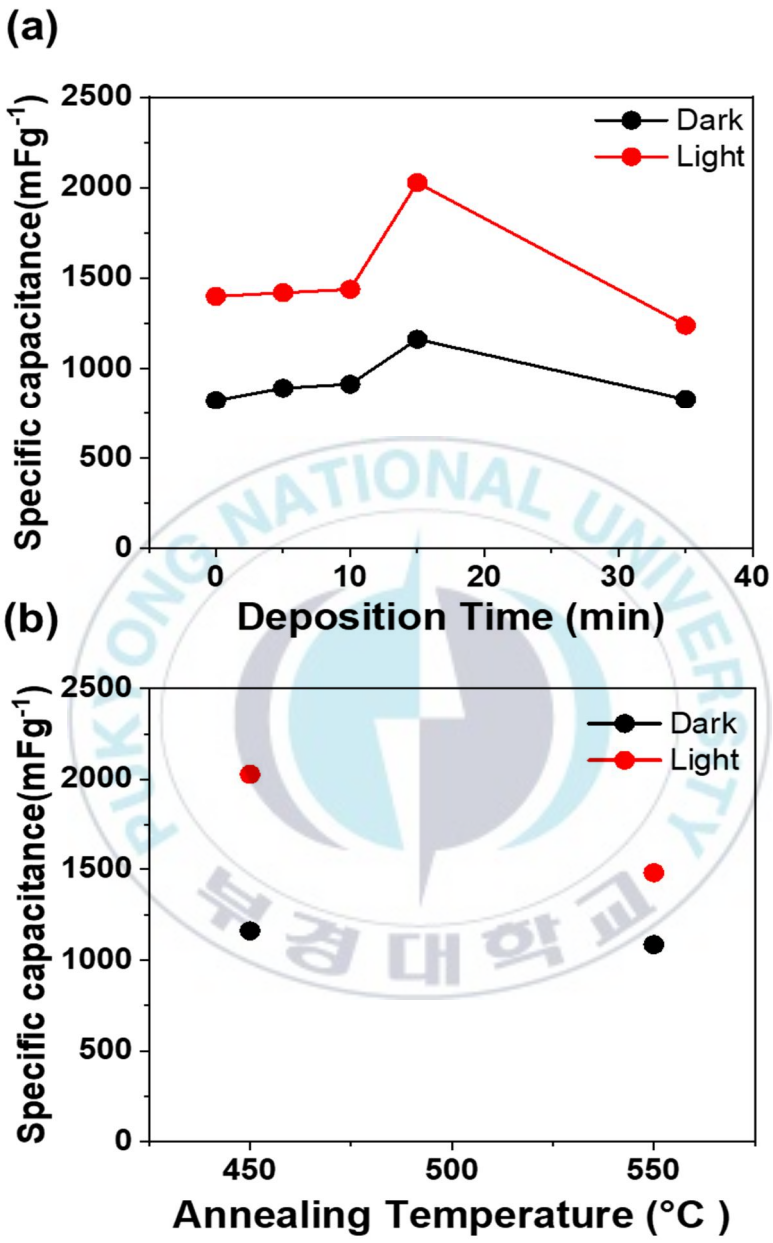

Figure 1. Specific capacitance by GCD measurement in the potential range of -1.4 to +0.8V (vs AC) at a current density of 8mAg^{-1} according to electrodeposition conditions (a) deposition time (b) annealing temperature

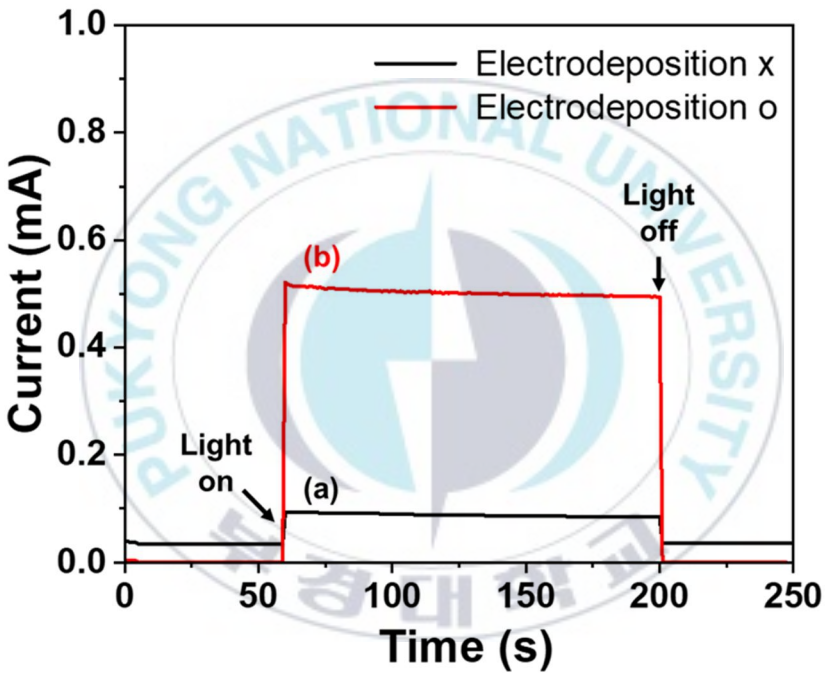

Figure 2. Photocurrent at 1.0V (vs. Ag/AgCl) (a) WO_3 (b) electrodeposited WO_3

2.2. Characterization and (photo) electrochemical measurements

Cell configurations were assembled by using the as-prepared WO_3 electrode (1cm x 1cm) as anode and graphite foil (Alfa, 1mm thick, 0.1cm x 0.1cm) as a cathode in a single quartz cell. Note that we use quartz cells due to light irradiation. 0.5M Li_2SO_4 solution in water is used for electrolyte. The pH of the solution was adjusted to 4.00 by adding H_2SO_4. The cell was purged with nitrogen gas for 30minutes prior to measurements and continuously purged in the electrolyte surface to remove oxygen during the reaction. For solar light irradiation, a solar simulator (1sun, AM 1.5G, Abet) was used as the light source.

WO_3 thin film was characterized by X-ray diffraction (XRD, PANalytical (X'Pert 3-Powder)) using Cu-Kα radiation.

The galvanostatic charge and discharge (GCD) measurements were performed using an electrochemical workstation (ZIVE SP1, WONATECH) in a two-electrode system containing 0.5M Li_2SO_4 pH 4.00 electrolyte (working volume: 45ml) under nitrogen atmosphere with WO_3 electrode as a working electrode, graphite foil as both counter and reference electrode. In addition, we observe the working electrode potential to the Ag/AgCl (3M NaCl) as a reference electrode by connecting the AUX line during the measurement, as shown in scheme 5.

Cyclic voltammetry (CV) was measured using a three-electrode system containing the same electrolyte solution (working volume: 45ml) under a nitrogen atmosphere.

The WO_3 electrode, Ag/AgCl (3M NaCl), and Pt wire were used as working electrode, reference electrode, and counter electrode, respectively. CV was carried out over a potential range of -0.6V to 0.6V (vs. Ag/AgCl) at a different scan rate ranging from 10 mvs^{-1} to 200 mvs^{-1} on an electrochemical workstation (Ivium N-stat, Ivium Technologies BV).

Electrochemical impedance spectroscopy (EIS) measurements were carried out in a three-electrode system using an electrochemical workstation (Metrohm Autolab PGSTAT204) under nitrogen atmosphere. The WO_3 electrode, Ag/AgCl (3M NaCl), and graphite foil were used as working electrode, reference electrode, and counter electrode, respectively.

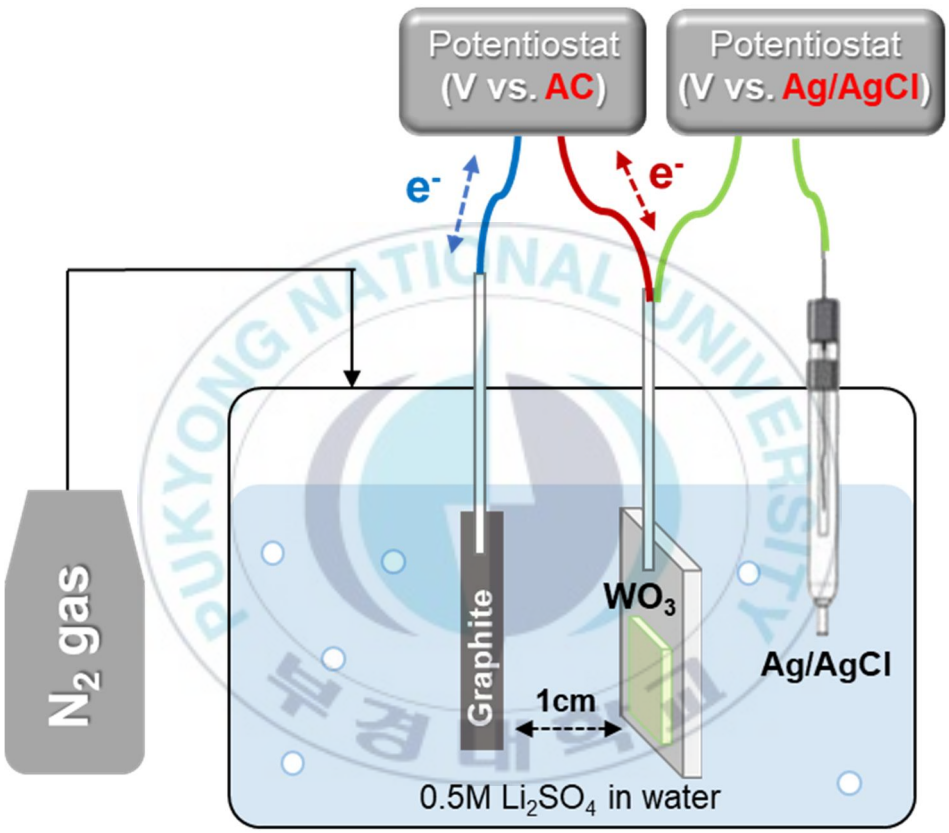

Scheme 5. Schematic illustration of the GCD measurement

3. Results and discussion

3.1. Electrochemical measurement

3.1.1. X-ray diffraction (XRD) measurements

The lithium ions intercalation in WO_3 occurs during the lithiation process. This process can simply be expressed by the following equation.[10,30]

$$WO_3 + xLi^+ + xe^- \rightarrow Li_xWO_3 \qquad (0 < x \leq 1) \qquad (1)$$

The intercalation of lithium ions is confirmed by XRD measurement, as shown in figure 3a. The as-prepared WO_3 is presented as a monoclinic structure, through the peaks with 2θ at 23.1°, 23.7°, 24.2° corresponding to the [002], [020], [200] directions.[31-33] Compared to the XRD pattern of the WO_3 before charge, new peaks appear after the lithiation and disappear after delithiation. This depicts that WO_3 exhibits good reversibility and electrochemical intercalation/extraction of lithium ions carried out well. The conversion of the WO_3 to Li_xWO_3 can also be confirmed by observing the dark blue coloration during lithiation[34], as shown in figure 3b. Thanks to these characteristics by photoelectrochromism, the degree of coloration can be allowed by the visualization of the lithiation state.[35]

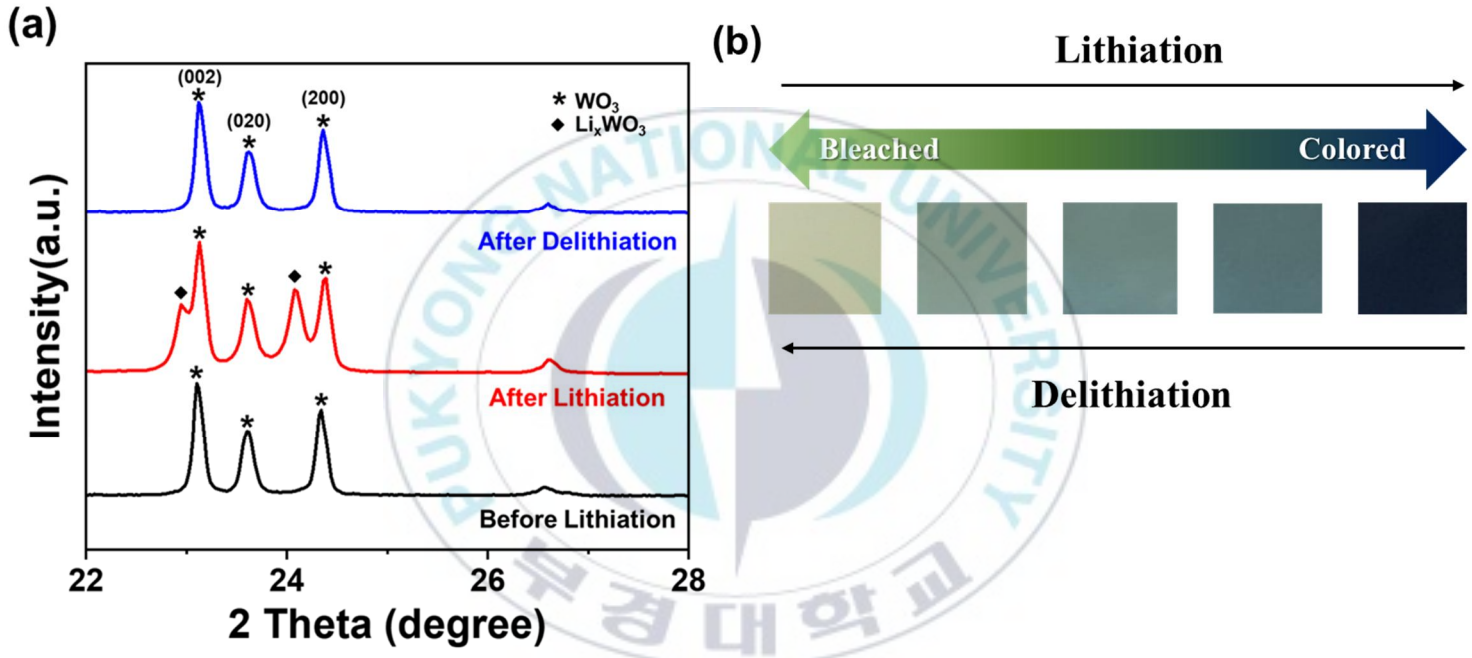

Figure 3. (a) XRD patterns change of WO_3 (b) color change in WO_3 electrode before and after lithiation/delithiation

3.1.2. Galvanostatic charge and discharge

Before galvanostatic charge and discharge (GCD) measurement, we should consider an electrochemical stability window of aqueous-based electrolyte[3,36] in order to set up the operating voltage range. Figure 4 is the pourbaix diagram of tungsten, which shows the WO_3 is stable below pH 4.00.[37,38] Accordingly, the pH of the 0.5M Li_2SO_4 electrolyte was set to 4.00. To determine the operating voltage range, we measured overall voltage profiles in 0.5M Li_2SO_4 pH 4.00 at 17mAg^{-1}. Figure 5 exhibit the voltage profiles when lithiation and delithiation are sufficiently performed. In addition, we evaluated the electrochemical stability window by linear sweep voltammetry (LSV). Figure 6 shows the onset potential of water oxidation and reduction occurring at 1.8V and -0.5V (vs. Ag/AgCl), respectively, and electrochemical stability window is achieved at 2.3V (vs. Ag/AgCl).

Based on the above results, GCD measurements were tested by dividing the range to determine the optimum operating voltage range, as shown in figure 7. As a result, we decided to set up the cell voltage range from -1.4V to 0.8V (vs. AC)

We carried out GCD measurements in the voltage range of -1.4V to +0.8V (vs. AC) at a current density of 17mAg^{-1}. Figure 8 shows the capacities were increased under light irradiation as compared to dark conditions. This result was interpreted as increased capacities due to the formation of photogenerated electrons by the photocatalytic properties of WO_3.

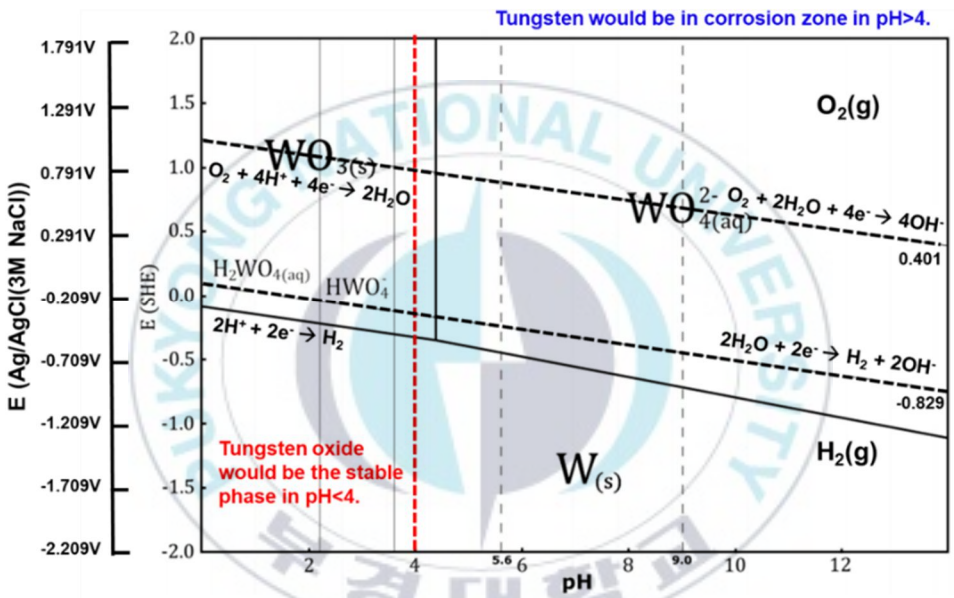

Figure 4. Pourbaix diagrams for W, dotted lines showing the reduction and oxidation equilibrium of water reproduced from reference [33]

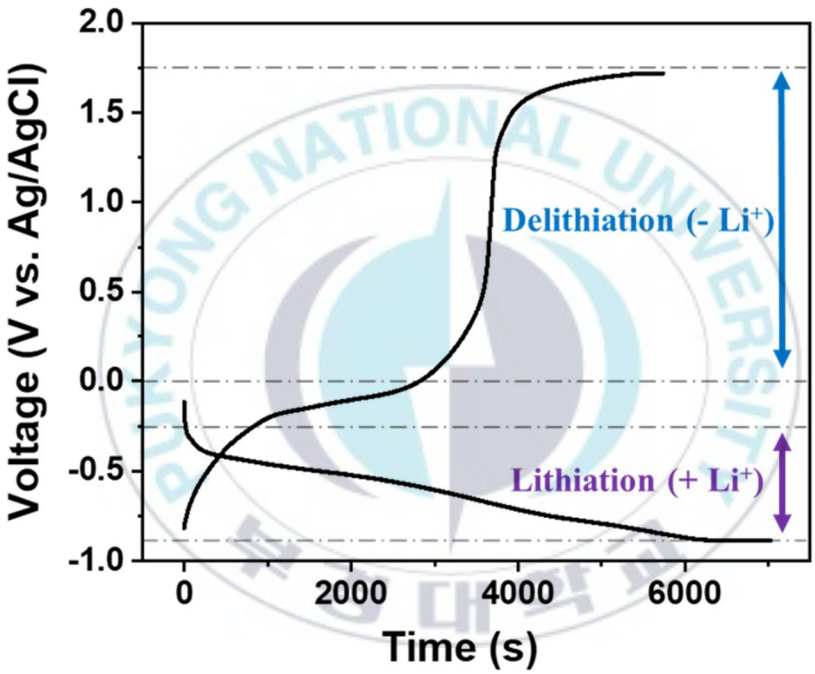

Figure 5. Lithiation/delithiation voltage profiles of WO_3 electrodes at 17mAg^{-1} in 0.5M Li_2SO_4 pH 4.00

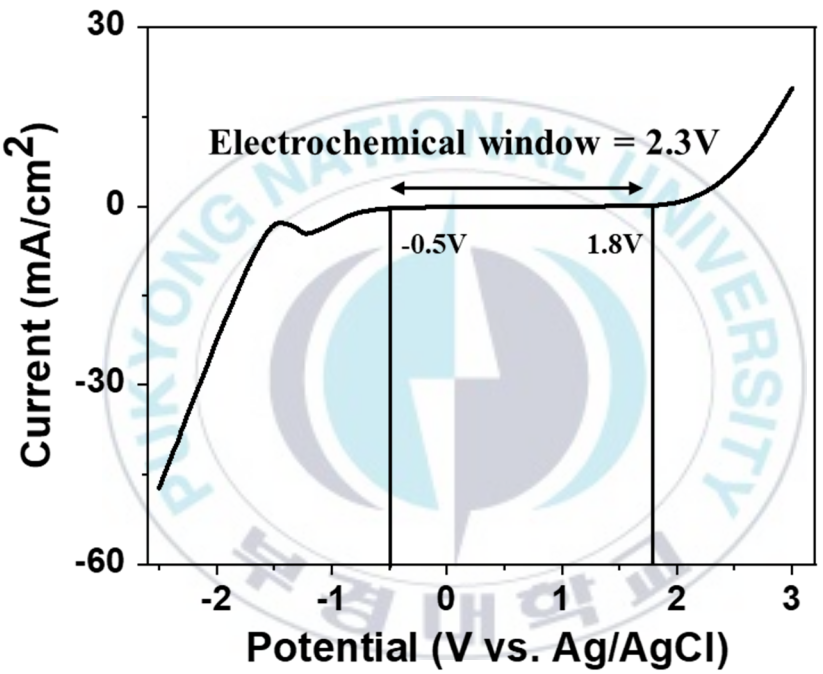

Figure 6. The electrochemical stability window of 0.5M Li_2SO_4 pH 4.00 in water measured by LSV

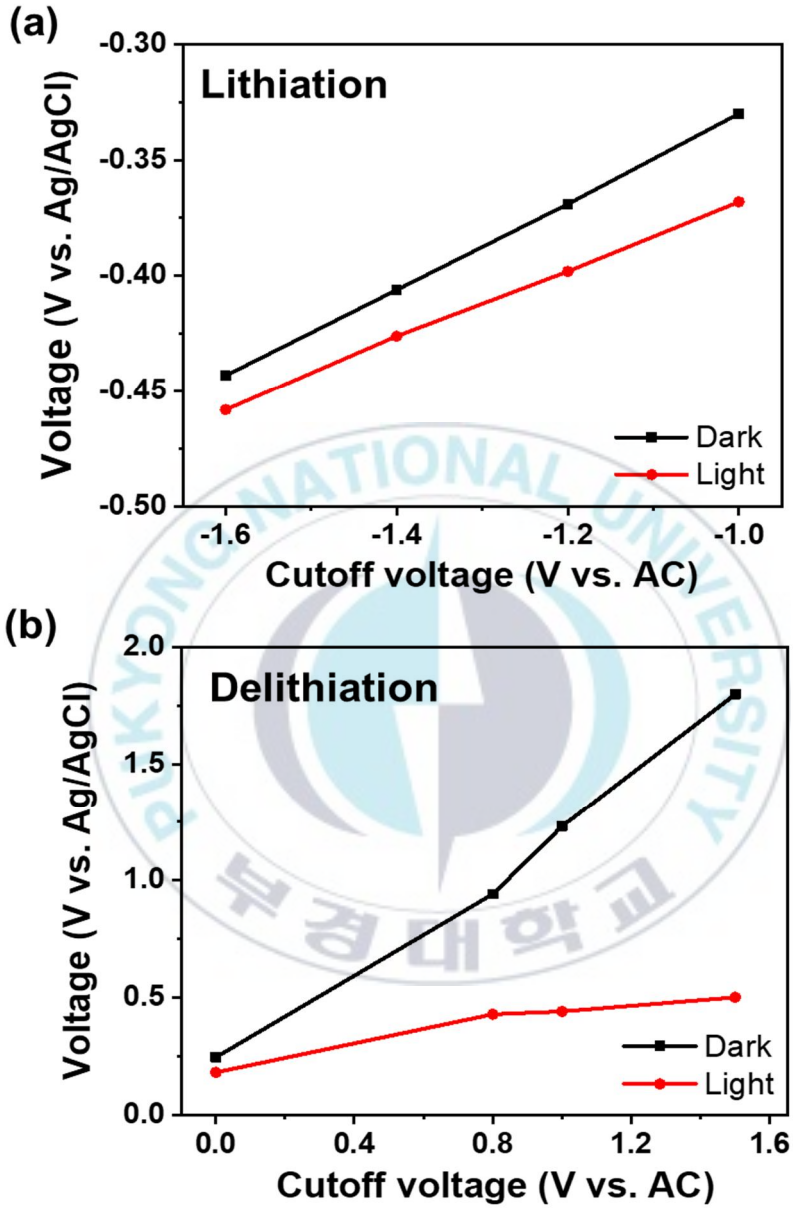

Figure 7. GCD measurements by dividing the cut-off range (a) lithiation cut-off voltage is -1.6V, -1.4V, -1.2V, -1.0V; delithiation cut-off voltage is fixed at 1.0V (vs. AC) (b) delithiation cut-off voltage is 0V, 0.5V, 0.8V, 1.0V, 1.5; lithiation cut-off voltage is fixed at-1.4V (vs. AC) at a current density of 17mAg^{-1}

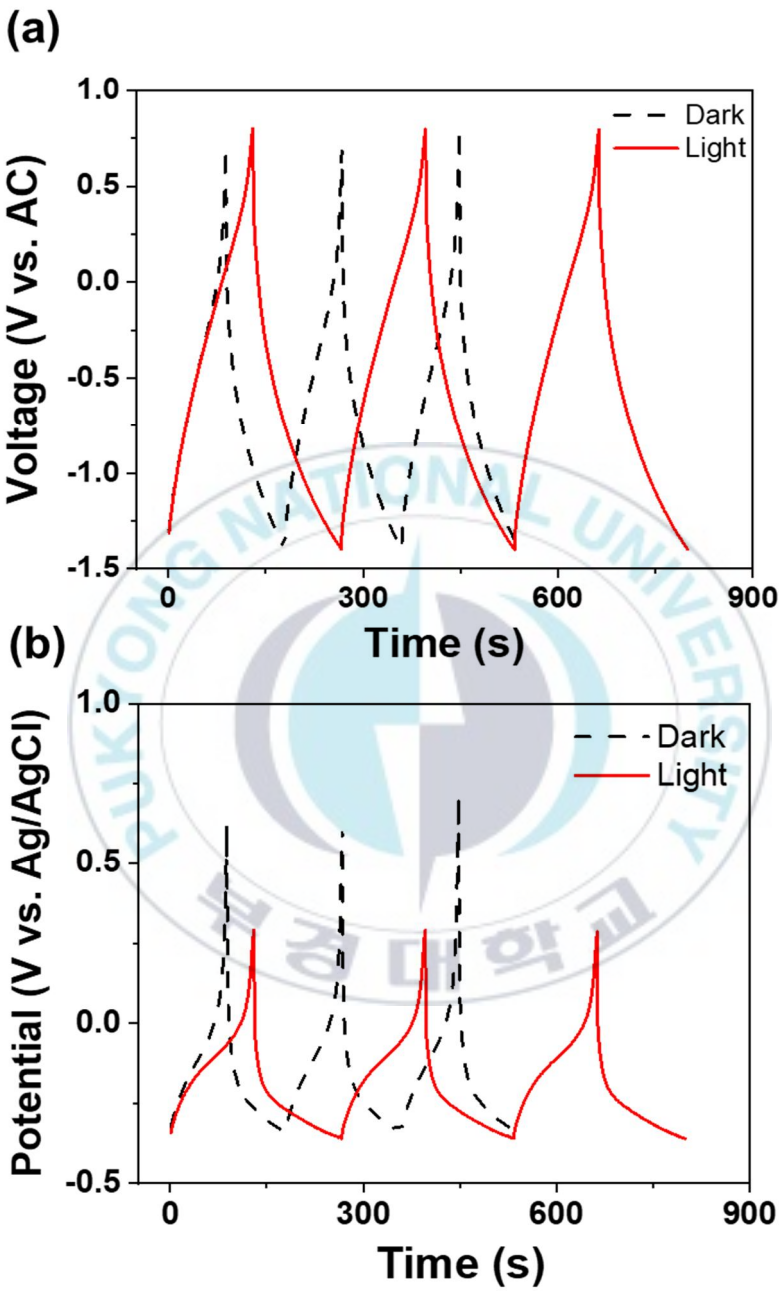

Figure 8. Lithiation/delithiation curves of WO_3 electrodes at a current density of 17mA g^{-1} (a) voltage (vs. AC) (b) potential (vs. Ag/AgCl)

3.1.3. Cyclic voltammograms measurements

To demonstrate electrochemical activity under light irradiation, we measured the cyclic voltammograms (CV) for WO_3. Figure 9a and 9b show CV curves of WO_3 electrodes at different scan rates in the potential range of -0.6V to +0.6V (vs. Ag/AgCl) for light and dark conditions, respectively. The area under CV curves was increased under the light irradiation case. This means that the total stored charge which arises from both faradaic and non-faradaic processes increase under light conditions.[39] With increasing scan rate, the shift of the cathodic peaks is not evident. The reason for this characteristic is that the WO_3 film has a broad distribution of energetically different intercalation sites.[40,41] On the other hand, the anodic peaks slightly shift to a positive potential, indicating the better electrochemical reversibility of the electrode reaction.[42]

The diffusion coefficients can be calculated from the Randles-Sevcik equation. The equation given without derivation is a below.

$$i_p = 0.4463nFAC\left(\frac{nF}{RT}\right)^{1/2}D^{1/2}v^{1/2} \qquad (2)$$

For one electron transfer at 25℃:

$$i_p = 2.69 \times 10^5 ACD^{1/2}v^{1/2} \qquad (3)$$

where i_p is the peak current (A), A is the active surface area of the electrode(cm^2), C is the concentration of active ion in the electrolyte ($molcm^{-3}$), D is the diffusion coefficient (cm_2s^{-1}), v is the scan rate (Vs^{-1}). Figure 10a and 10b show a plot of peak current (I_p) versus the square root of the scan rate ($v^{1/2}$).[1,42,43] The values of diffusion

coefficient (D) can be obtained by calculating from equation (3). That is, the slope is equal to $2.69 \times 10^5 ACD^{1/2}$. Through the calculations, the values of diffusion coefficient (D) for oxidation (anodic) and reduction (cathodic) under dark are 2.90×10^{-10} and 1.38×10^{-9}, respectively. Under light irradiation conditions, the values of D for oxidation and reduction are 2.31×10^{-9} and 5.56×10^{-9}, respectively. Therefore, WO_3 performs further convenient intercalation/extraction process for lithium ions under light irradiation.[9,43]

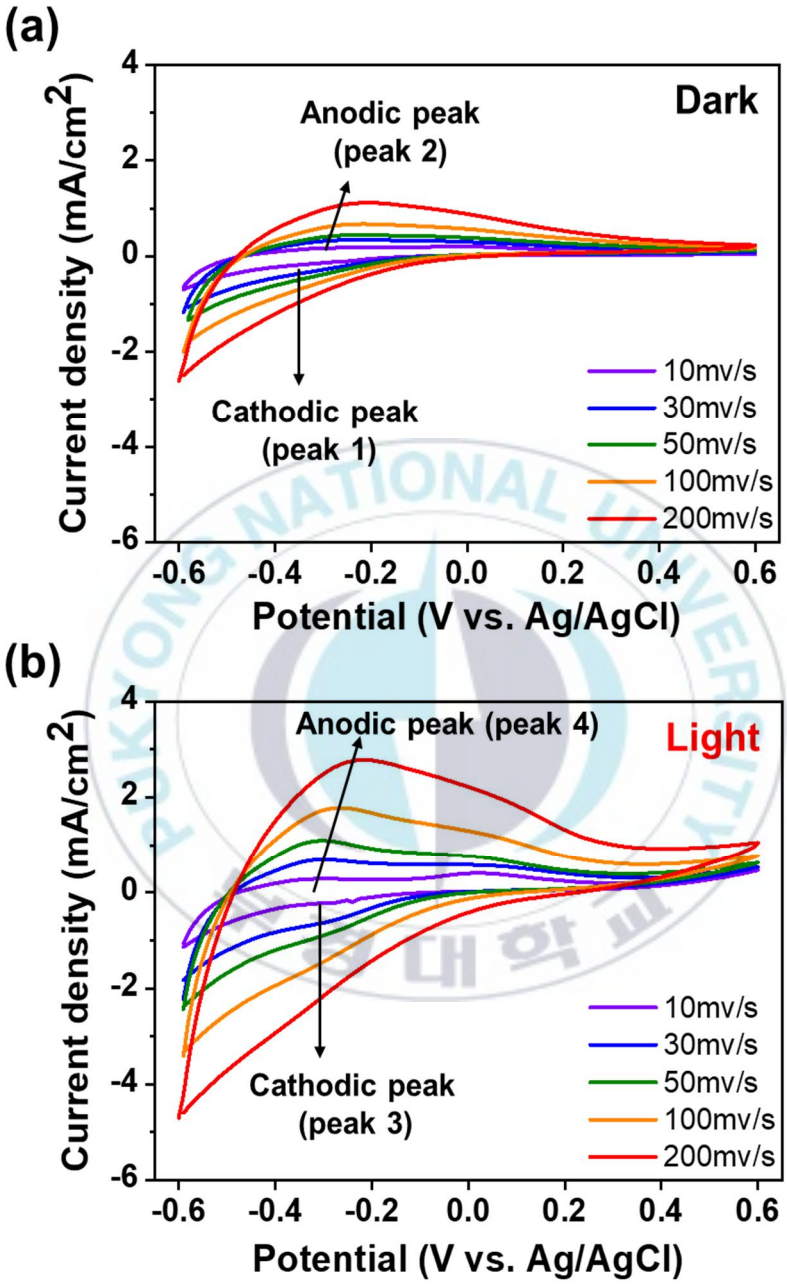

Figure 9. CV curves of WO_3 electrode at different scan rates under (a) dark (b) light irradiation

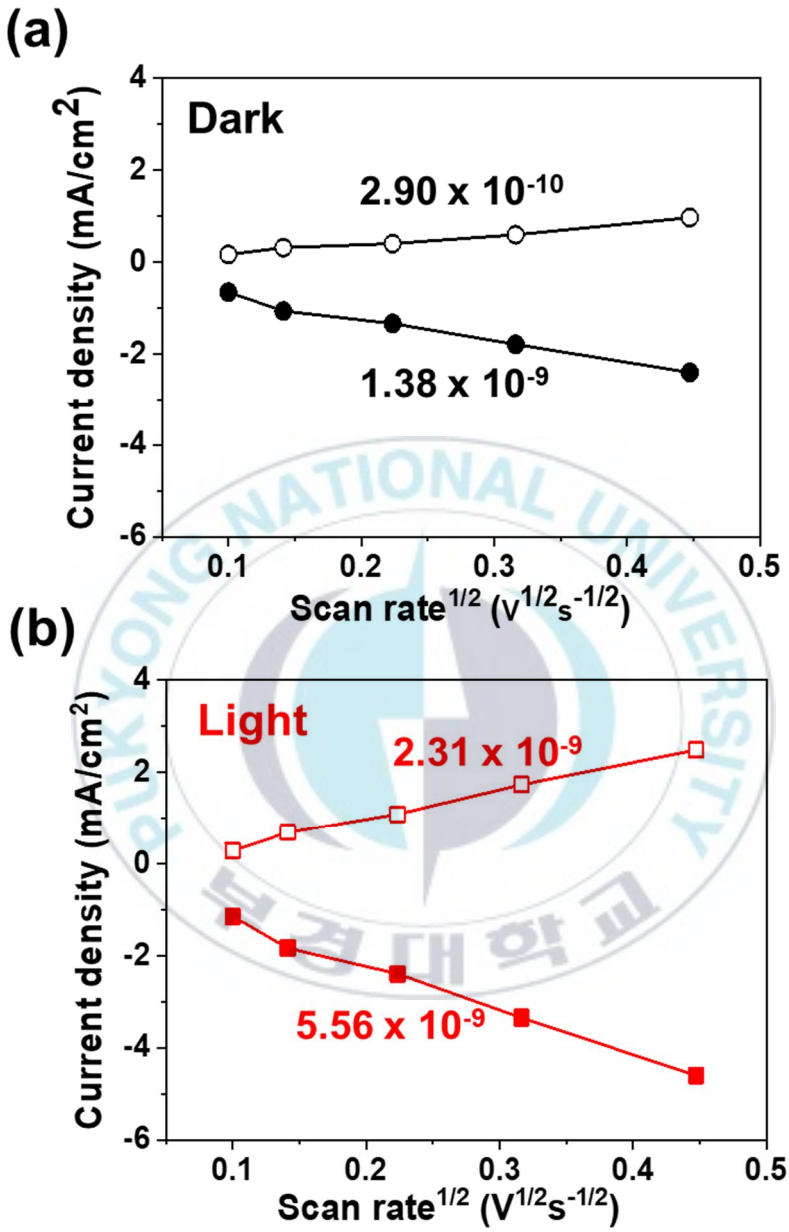

Figure 10. Corresponding linear fitting for the relationship between redox peak and square root of scan rate from CV curves under (a) dark (b) light irradiation

3.1.4. Electrochemical impedance measurements

To investigate the effect of photogenerated electrons in electrochemical process, we carried out electrochemical impedance spectroscopy (EIS) measurements. EIS is a well-established technique to investigate kinetics for electrochemical processes occurring in batteries during lithiation and delithiation process[44] and provides detailed information for the interfaces of electron transport and charge transfer characteristics.[45]

EIS measurements were tested under dark and light conditions. The voltage bias was set up at 0.5V with a frequency range of 100kHz to 100 Hz for delithiation and amplitude voltage of 10mV. Figure 11b shows the Nyquist plot of WO_3, which corresponds to a high-frequency region associated with charge transfer and a low-frequency region related to Warburg impedance, which indicates the diffusion process of ions at the interface between the electrolyte and active material.[9,46]

The impedance is analyzed by an equivalent electrical circuit model, as in illustrated in figure11a and the parameters are tabulated in table 1. In the equivalent electrical circuit model, R_s represents electrolyte resistance, R_{ct} is faradaic charge transfer resistance, C_{dl} double-layer capacitance, W is Warburg impedance, and C_{ps} is pseudocapacitance.[12,44-47] As shown in figure 11b and table 1, W, C_{dl}, and C_{ps} gradually increased, while R_{ct} decreased under continuous light irradiation.

Therefore, increased C_{dl} and C_{ps} indicate the surface capacitance enhance, and decreased R_{ct} reveals electron transport ability enhanced due to the photogenerated electrons.[9]

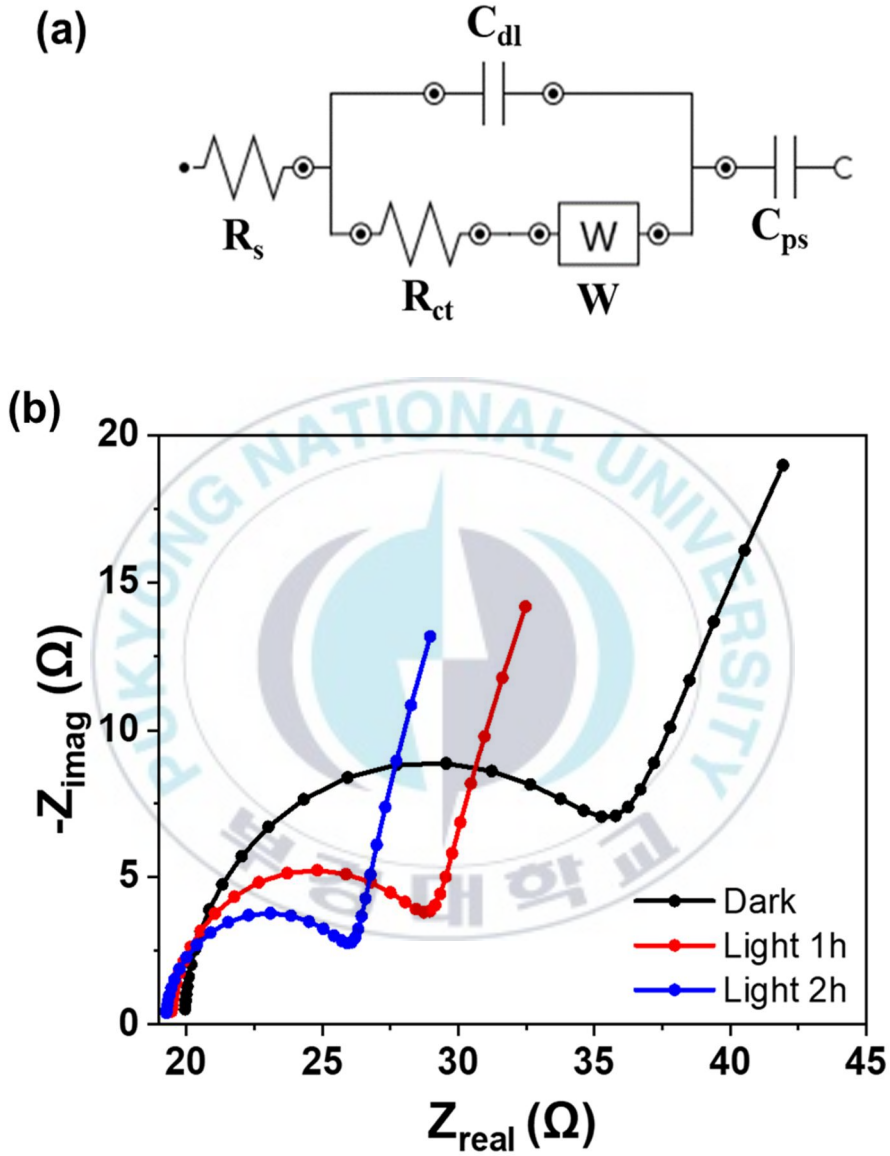

Figure 11. (a) Equivalent electrical circuit model for Nyquist plot (b) Nyquist plots (Z_{real} vs. $-Z_{imag}$) of WO_3 at 0.5V (vs. AC) under dark and light conditions

	$R_s(\Omega)$	R_{ct} (Ω)	W	C_{dl} (μF)	C_{ps} (μF)
Dark	19.8	14.7	3.86m	2.89	150
Light 1h	1.92	8.26	6.07m	3.62	165
Light 2h	1.91	6.34	8.89m	4.02	174

Table 1. Values of parameters from the Nyquist plot in figure 11b using the equivalent circuit model in figure 11a

3.2. The working mechanism of the solar energy-assisted lithium-ion battery

3.2.1. Kinetic analysis of the electrochemical behavior of WO_3

The photogenerated electrons from WO_3 enhance the capacity by participating in the intercalation of lithium ions, and improving the surface capacitance of electrodes. We analyzed the kinetics of the WO_3 electrodes to investigate which of the intercalation/extraction and surface capacitance effects by photogenerated electrons predominated.

We considered three charge-storage mechanisms as reported previously: (1) the diffusion-controlled faradic contribution from the lithium ions intercalation process, (2) the faradaic contribution from charge transfer with surface from the charge-transfer process, referred to as pseudocapacitance, (3) the non-faradaic contribution from the double layer.[48] These effects can be largely separated into surface-controlled capacitance effect, and diffusion-controlled intercalation effect. To distinguish between the above effects, we performed the cyclic voltammetry at various rates. According to the equation,

$$\mathrm{i} = \mathrm{a}v^{b} \qquad (4)$$

$$\log i = b \log v + \log a \qquad (5)$$

where i is the peak current (A), a and b (referred to b-values) are adjustable parameters, and v is the scan rate (Vs^{-1}). The b-values can be reflected the charge-

storage mechanisms of lithium ions. If the calculated b-values are approaching 0.5, it represents the diffusion-controlled intercalation effect. In contrast, if the calculated b-values are close to 1.0, it represents a surface-controlled capacitance effect.[49,50] As shown in figure 9a and 9b, CV curves display anodic peaks and cathodic peaks under dark and light irradiation conditions. We calculated b-values (the slope of the plot of log *i* vs. log *v*) according to equation (5). b-values of anodic peaks under dark and light conditions are 0.60 and 0.77, respectively, demonstrating that the surface-controlled capacitance effect predominates the diffusion-controlled intercalation effect. On the other hand, b-values of cathodic peaks under dark and light are 0.51 and 0.55, respectively, indicating the diffusion-controlled intercalation effect predominates the electrode reaction. Overall, in both anodic and cathodic peaks, the surface-controlled capacitance effect was expanded more under the light conditions. To investigate the above results in more detail, we analyzed the contribution of the surface-controlled capacitance and the diffusion-controlled intercalation effects at a specific potential. According to the equation, [1,39,48,51,52]

$$\mathrm{i(V)} = k_1 v + k_2 v^{1/2} \qquad (6)$$

$$\mathrm{i(V)}/v^{1/2} = k_1 v^{1/2} + k_2 \qquad (7)$$

where i(V) is the current response at a fixed potential (A), $k_1 v$ and $k_2 v^{1/2}$ represent the contribution of the surface-controlled capacitance effect and the diffusion-controlled intercalation effect, and *v* is the scan rate (Vs^{-1}). Following the data in figure 9a and 9b, $k_1 v$ and $k_2 v^{1/2}$ determine the plot of the scan rate dependence of the current at a

specific potential using equation (7). The calculated data are tabulated in table 2 and table 3. As shown in table 2 and table 3, the contribution of the diffusion-controlled intercalation effects further takes up than the contribution of surface-controlled capacitance effects. However, the surface-controlled capacitance also gets a small share of the contribution, and the light effect is more sensitive in the surface-controlled capacitance effects. Therefore, these results clearly demonstrate that photogenerated electrons from WO_3 contribute to the surface-controlled capacitance effect along with the diffusion-controlled intercalation effect.

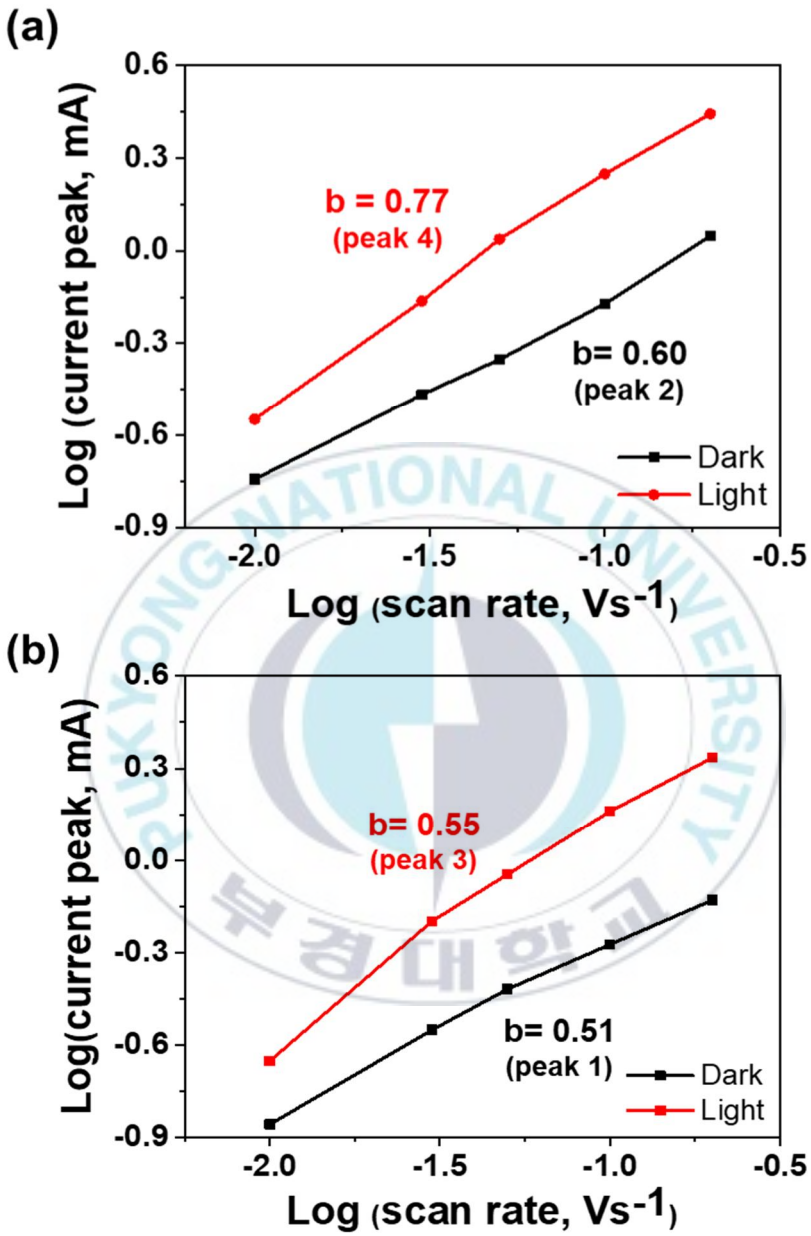

Figure 12. Relationship between log (peak current) and log (scan rate) under the dark and light conditions (a) anodic (delithiation), (b) cathodic (lithiation)

(a)

Anodic	Dark	Light	Dark	Light
scan rate (mV/s)	Surface capacitive effects (k_1v)	Surface capacitive effects (k_1v)	Diffusion-controlled Li^+ intercalation ($k_2v^{1/2}$)	Diffusion-controlled Li^+ intercalation ($k_2v^{1/2}$)
10	0.019	0.095	0.160	0.230
30	0.057	0.286	0.278	0.399
50	0.095	0.477	0.358	0.515
100	0.190	0.955	0.507	0.728
200	0.381	1.910	0.717	1.029

(b)

Cathodic	Dark	Light	Dark	Light
scan rate (mV/s)	Surface capacitive effects (k_1v)	Surface capacitive effects (k_1v)	Diffusion-controlled Li^+ intercalation ($k_2v^{1/2}$)	Diffusion-controlled Li^+ intercalation ($k_2v^{1/2}$)
10	0.006	0.068	0.146	0.214
30	0.018	0.205	0.253	0.370
50	0.030	0.342	0.326	0.478
100	0.060	0.685	0.461	0.676
200	0.121	1.370	0.653	0.956

Table 2. The contribution of the surface-controlled capacitance and the diffusion-controlled intercalation effects at (a) anodic (delithiation), (b) cathodic (lithiation)

(a)

Anodic	Dark	Light	Dark	Light
scan rate (mV/s)	Surface capacitive effects (k_1v)	Surface capacitive effects (k_1v)	Diffusion-controlled Li^+ intercalation ($k_2v^{1/2}$)	Diffusion-controlled Li^+ intercalation ($k_2v^{1/2}$)
10	10.625	29.318	89.375	70.682
30	17.076	41.807	82.924	58.193
50	21.001	48.119	78.999	51.881
100	27.323	56.741	72.677	43.259
200	34.712	64.974	65.288	35.026

(b)

Cathodic	Dark	Light	Dark	Light
scan rate (mV/s)	Surface capacitive effects (k_1v)	Surface capacitive effects (k_1v)	Diffusion-controlled Li^+ intercalation ($k_2v^{1/2}$)	Diffusion-controlled Li^+ intercalation ($k_2v^{1/2}$)
10	3.967	24.275	96.033	75.725
30	6.676	35.702	93.324	64.298
50	8.455	41.753	91.545	58.247
100	11.552	50.341	88.448	49.659
200	15.591	58.910	84.409	41.090

Table 3. The percentage of the surface-controlled capacitance and the diffusion-controlled intercalation effects at (a) anodic (delithiation), (b) cathodic (lithiation)

3.2.2. Light irradiation effects

We observed an inappreciable difference between lithiation and delithiation under light effects, as shown in table 2 and table 3. To investigate the above phenomenon in more detail, we carried out GCD measurements under divided light conditions in the voltage range of -1.4V to +0.8V (vs. AC) at a current density of 17mAg^{-1}. The specific capacitance from GCD is given by the following equation.

$$C_S = \frac{I \times t}{V \times m} \qquad (8)$$

where I is current density(mA), t is time(s), V is cell voltage(V), m is mass loading (g) of active electrode material.

As a result, we figured out three facts. First, the specific capacitance was increased significantly under continuous light irradiation rather than intermittent light irradiation. Secondly, we observed the effect of light is appreciably increased in the delithiation process compared to the lithiation process. This phenomenon can be explained by the band bending for WO_3, which is an n-type semiconductor, and electrochemical electrons flow. In the lithiation process, the electron-hole recombination occurs frequently due to the rich electrochemical electrons. On the other hand, in the delithiation process, photoelectrons can be supported by convenient extraction of lithium ions due to the match of electrochemical electrons flow and photogenerated electrons flow by band bending of WO_3, as shown in scheme 6b. Thirdly, figure 13a shows the capacitances were maintained continuously under intermittent light irradiation, neither reduced nor further increased. This means

accumulated photogenerated electrons can affect next reaction. The presence of accumulated photogenerated electrons was demonstrated by the negative shift of WO_3 working potential, as shown in figure 14. WO_3 remains rich in electrons due to accumulated photogenerated electrons by light irradiation, indicating enhanced capacitance by light irradiation maintained under dark, and even a slight change of WO_3 working potential can perform convenient intercalation/extraction of lithium ions. Also, the capacities were not further increased because Li_xWO_3, which is a charged state, has no photo-sensitivity.

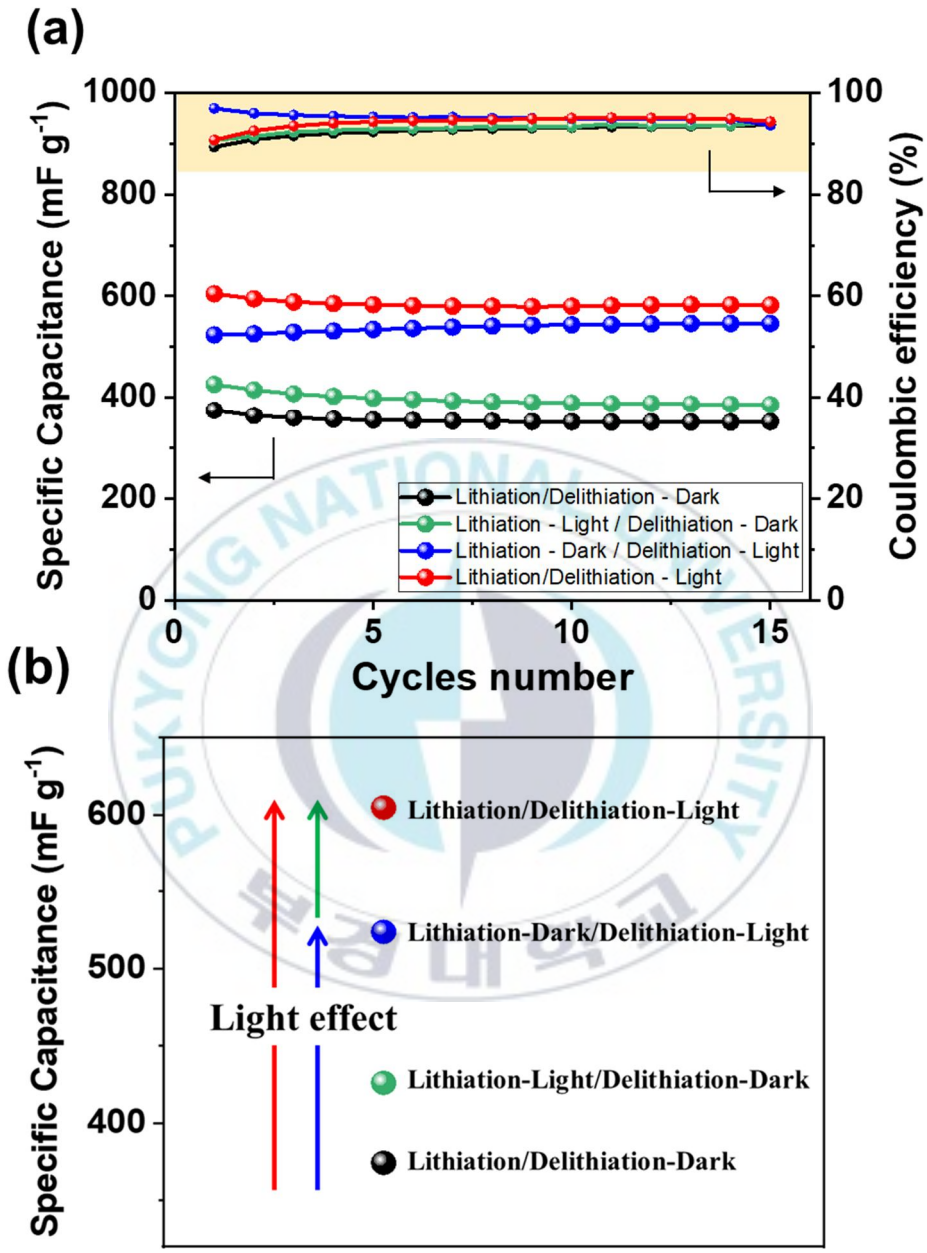

Figure 13. (a) The specific capacitance and coulombic efficiency under continuous and intermittent light irradiation (b) the specific capacitance in expanded scale

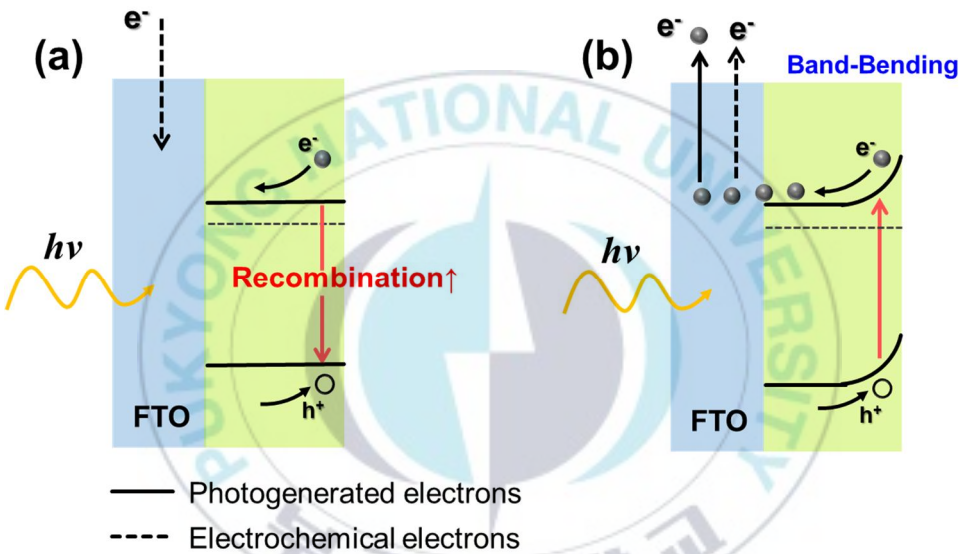

Scheme 6. Schematic illustration of the band-bending of WO_3 under light irradiation during (a) lithiation (b) delithiation

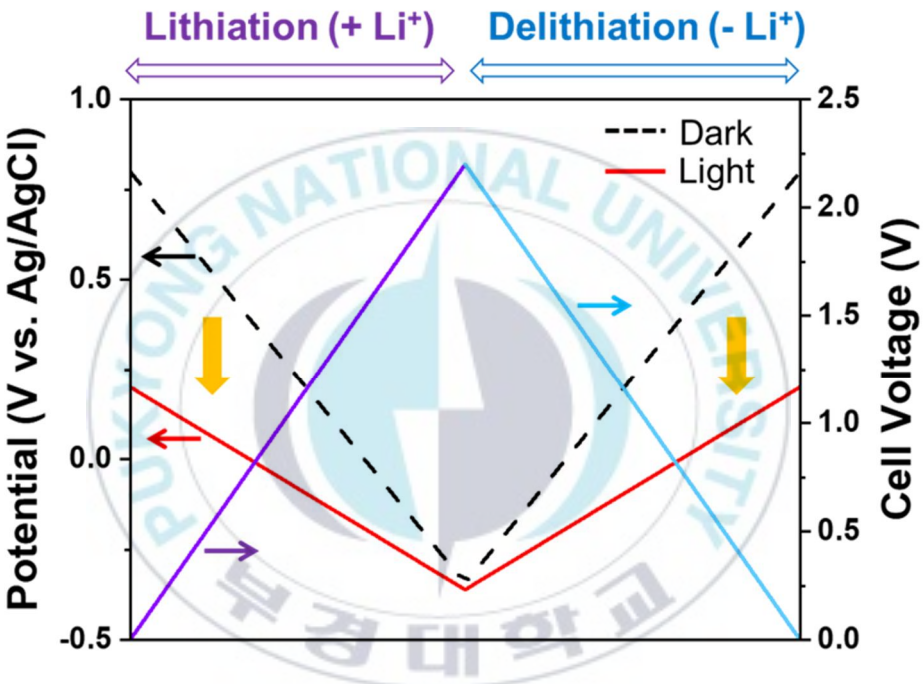

Figure 14. The negative voltage shift of WO_3 electrodes at a current density of 17mA g^{-1}

3.2.3. Lithium ion incorporation energy barriers on WO_3

To demonstrate the photogenerated electron effect during lithium ions intercalation, the energy barriers of lithium ion incorporation into WO_3 (001) surface are calculated using density functional theory (DFT) calculations, as shown in figure 15. The photoexcitation of WO_3 system was described with excessive electrons into WO_3(001) slab system. The WO_3(001) slab in charge neutrality has incorporation energy barrier of 99meV/atom, while negatively charged slabs (q=-1, -2, -3) have no energy barriers for the incorporations on the surface. In most of oxide anode materials, surface incorporation barriers are higher than diffusion energy barriers in bulk. Therefore, excessive charge on WO_3(001) anode can accelerate lithium ions intercalation process.

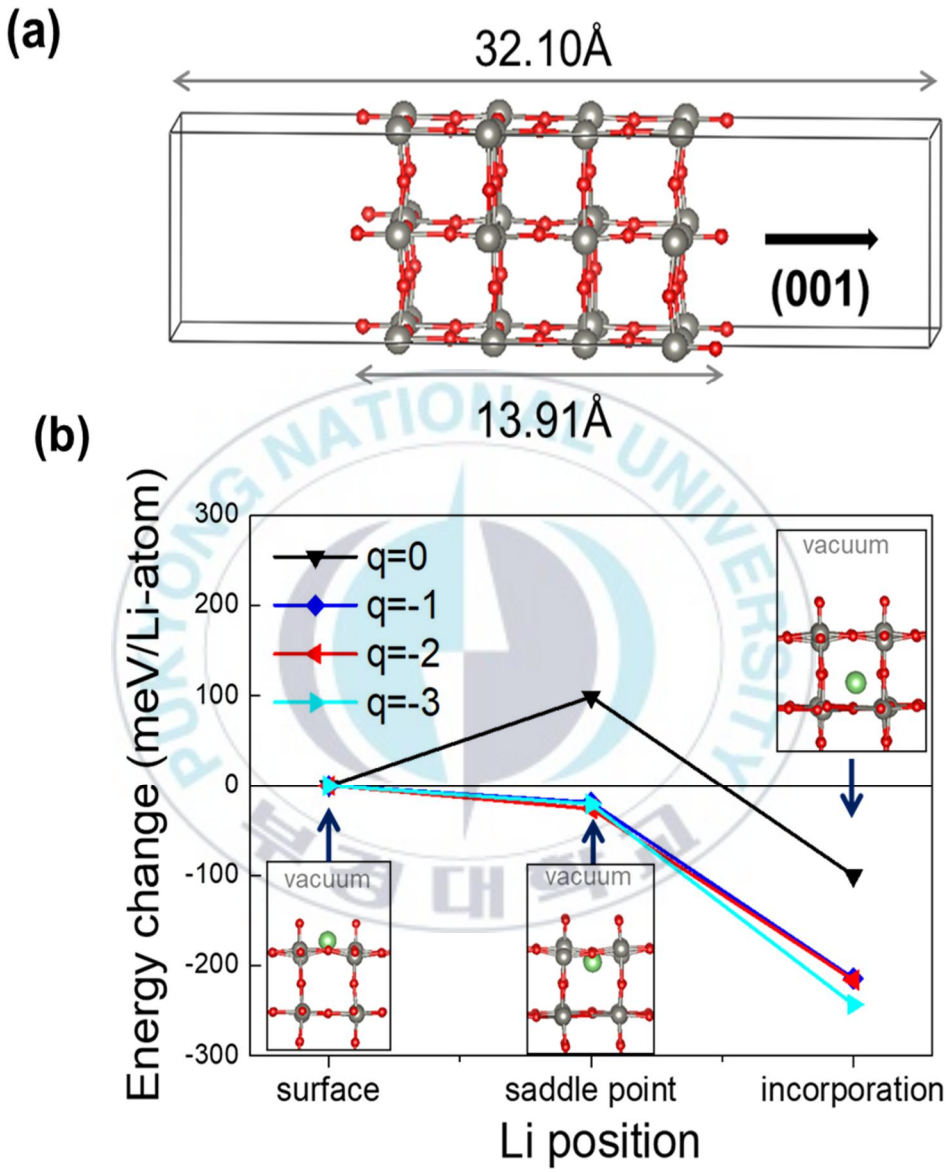

Figure 15. (a) WO_3 (001) slab system (b) the relationship between Li position and energy change to lithium-ion incorporation

3.3. Electrochemical performance

3.3.1. Rate performance

We carried out galvanostatic charge and discharge at a different current density to demonstrate the electrochemical performance of the solar energy-assisted lithium-ion battery. As shown in figure 16, the specific capacitances were increased at the current density 8, 13, 14, 17, 33, 50, 83, 133, and 167mAg^{-1} under light irradiation conditions due to the contribution of the photogenerated electrons. When added isopropyl alcohol (IPA) as a hole-scavenger, which restricts photogenerated electron-hole pair recombination, the capacitances were remarkably increased. This result demonstrates likewise that the origin of the improved capacity is the photogenerated electron, which was also confirmed earlier. Furthermore, when the current density reached 8mAg^{-1}, the specific capacitance was fully recovered to the initial value. This means the WO_3 crystal structures maintained and high stability and reversibility during lithiation/delithiation.[53]

We also analyzed the electrochemical performance under organic electrolyte (1.0 M LiPF6 in EC/DMC=50/50 (v/v), Sigma Aldrich) conditions, which are widely used in the commercial battery system. The experiment was conducted under the same conditions as the above, except for electrolyte. Figure 17 shows that the proposed battery also performs a high-rate performance in organic electrolytes. As shown in figure 18, the same result was obtained when we carried out the change of the area

of a counter electrode. Therefore, WO_3 was employed as an attractive anode material with stable rate performance of lithium ions intercalation/extraction and high-efficiency retention under light irradiation.

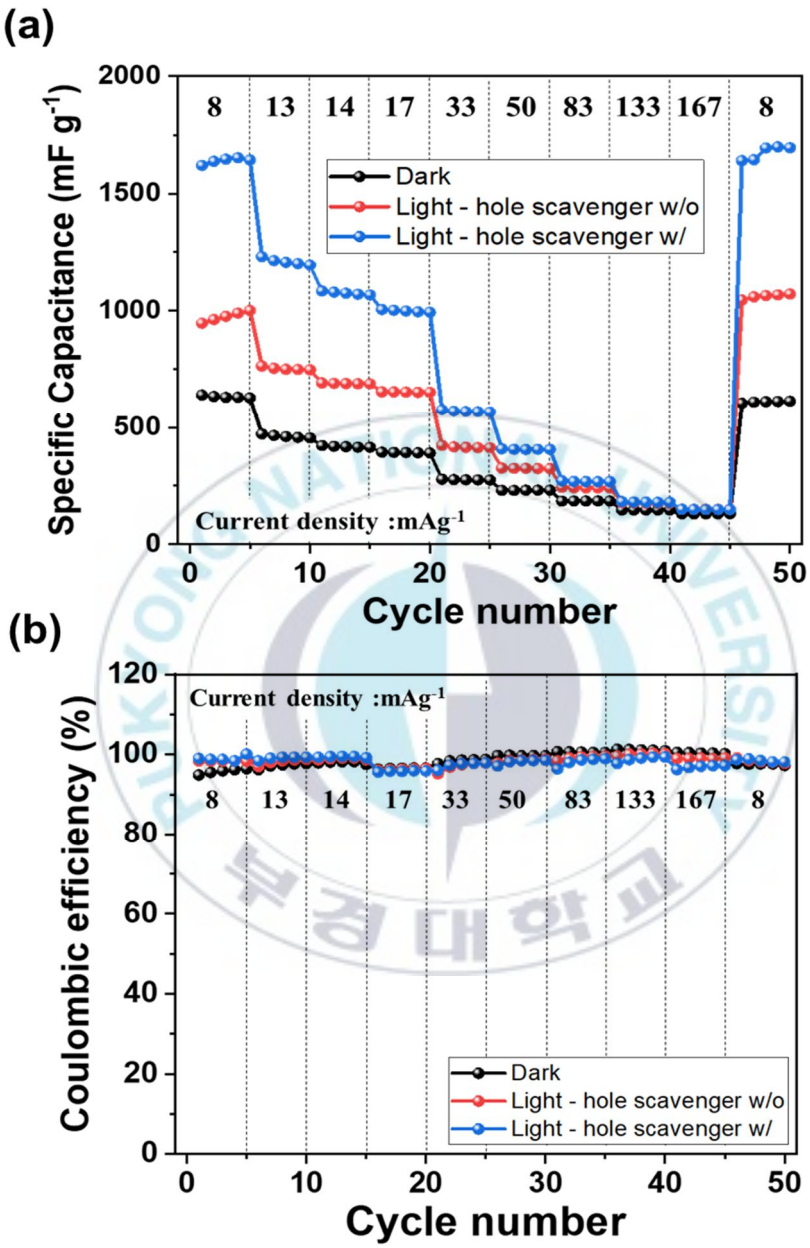

Figure 16. (a) Rate performance (b) coulombic efficiency of WO_3 in aqueous electrolyte (0.5M Li_2SO_4 pH 4.00) at a current density from 8mAg^{-1} to 167mAg^{-1}

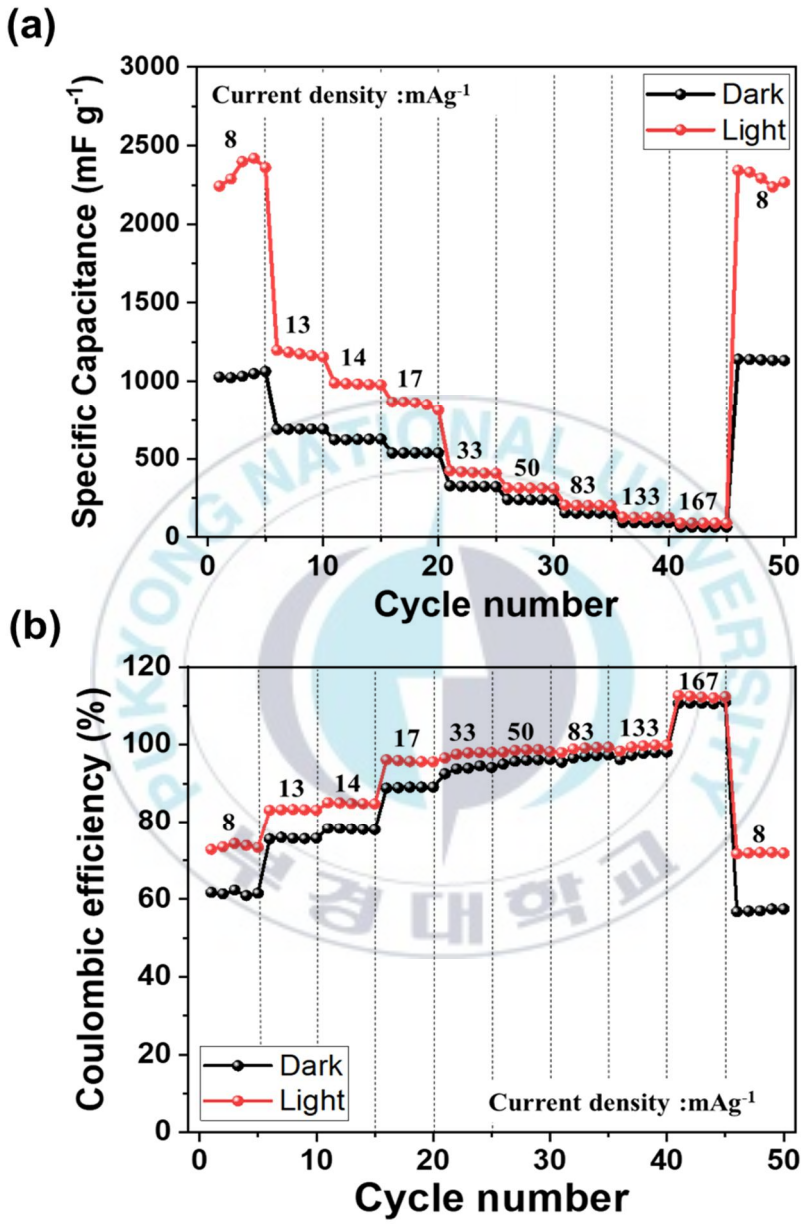

Figure 17. (a) Rate performance (b) coulombic efficiency of WO_3 in organic electrolyte (1M $LiPF_6$ EC/DMC) at a current density from 8mAg^{-1} to 167mAg^{-1}

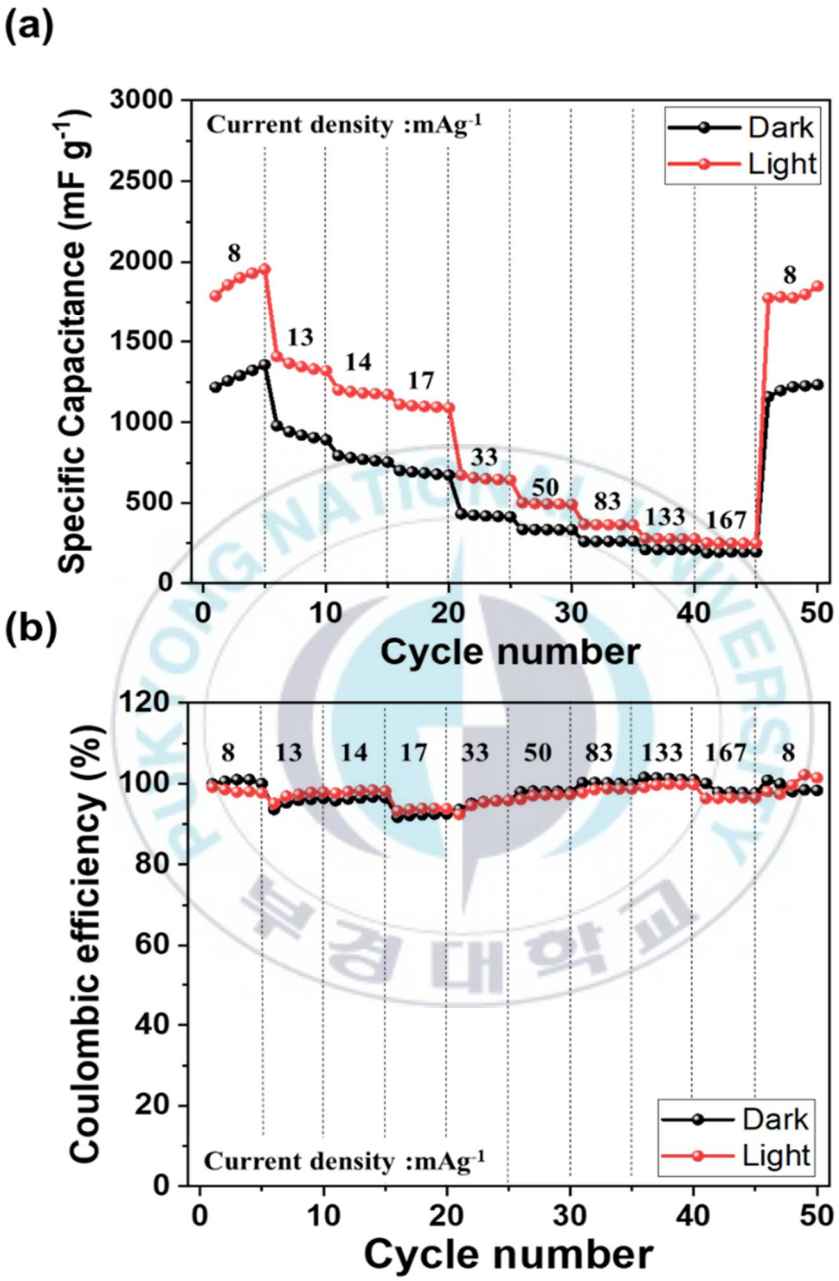

Figure 18. The counter electrode area (0.2cm x 0.2cm) change (a) rate performance (b) coulombic efficiency of WO_3 in aqueous electrolyte (0.5M Li_2SO_4 pH 4.00) at a current density from 8mAg^{-1} to 167mAg^{-1}

3.3.2. Long-term cycling performance

We evaluated the long-term performance at 17mAg^{-1} under dark and light conditions. As shown in figure 19, the average lithiation specific capacitances of WO_3 are 356mAg^{-1} and 522mAg^{-1} under dark and light conditions, respectively. Also, the coulombic efficiency was retained over 96%.

We carried out the EIS before and after the cycles. The voltage bias was set up open-circuit voltage (OCV) with a frequency range of 100kHz to 10 Hz and an amplitude voltage of 10mV. Figure 20 shows EIS measurements before and after cycles. After 500cycles, the R_s exhibited an increase under dark while the R_s depicted a decrease under light. This depicts that the photogenerated electrons assist convenient intercalation/extraction of lithium ions without drastic changes in WO_3 working potential, resulting in the prevention of the aging phenomenon of the battery. The semicircles, which is charge transfer resistance (R_{ct}), shrunk prior to the cycles. In particular, the charge transfer resistance after 500 cycles under light irradiation was observed to be lower as compared to the dark conditions. These results exhibit higher electroactivity for lithium ions storage under light irradiation.

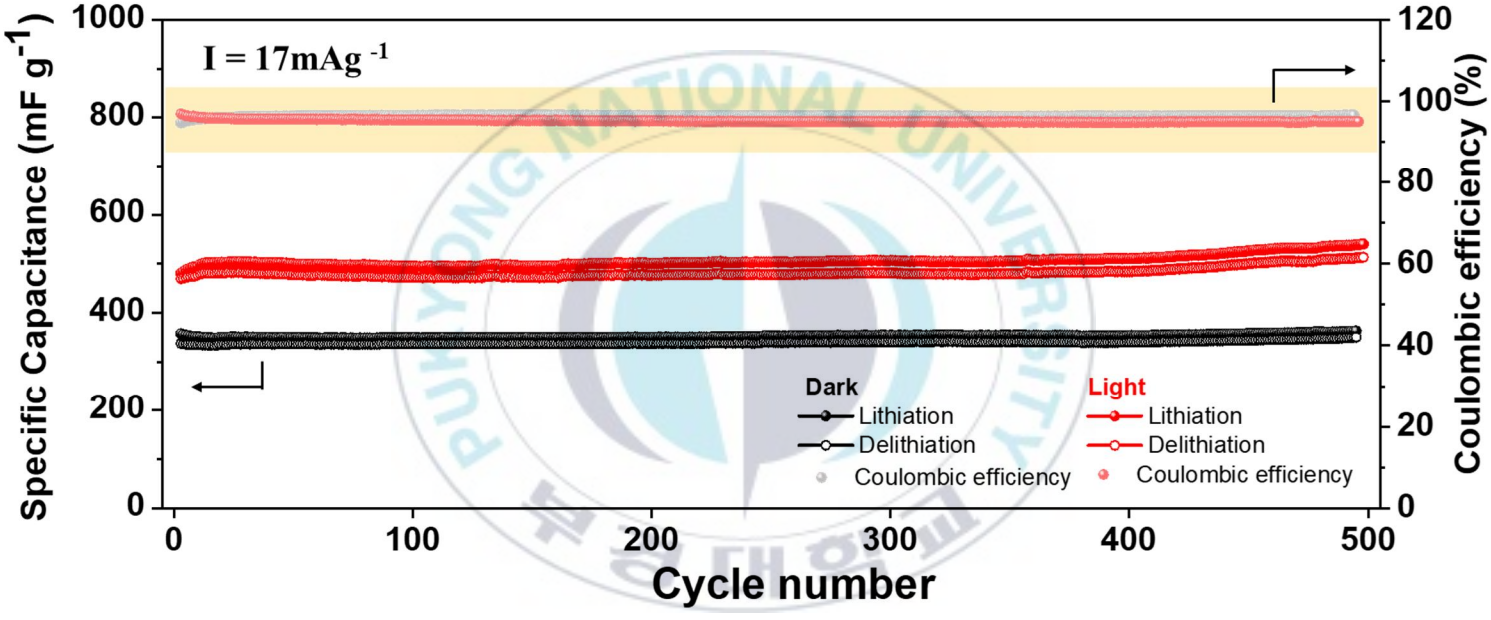

Figure 19. Long-term performance of WO_3 by GCD measurement at 17mAg^{-1} under dark and light

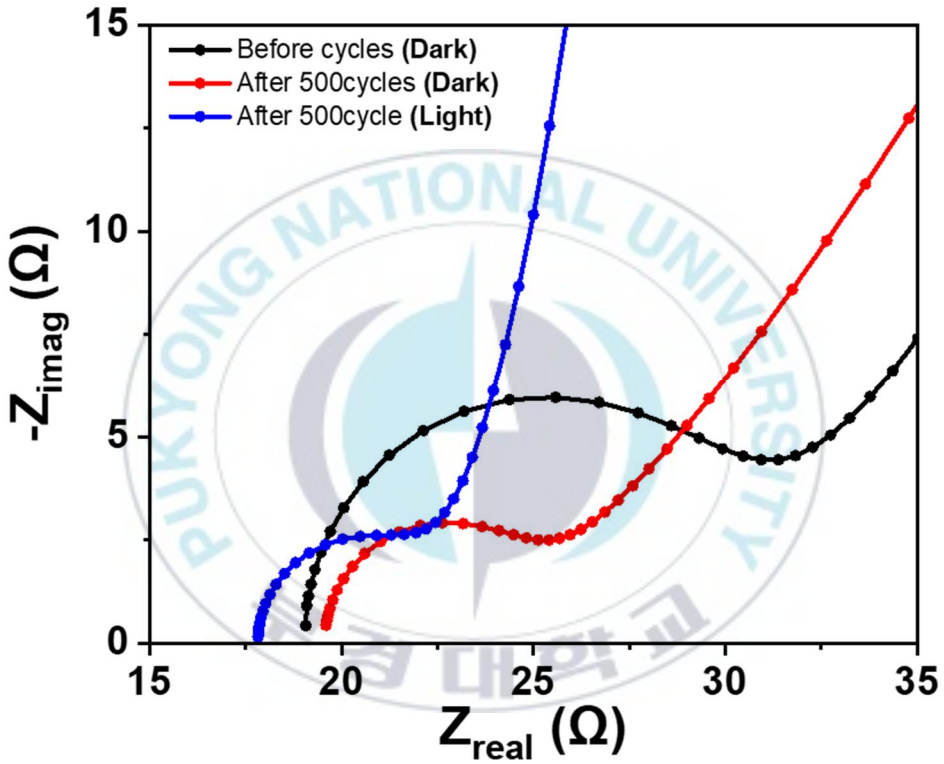

Figure 20. The Nyquist plots (Z_{real} vs. $-Z_{imag}$) of WO_3 at OCV before and after cycles

	R_s (Ω)	R_{ct} (Ω)	W	C_{dl} (μF)	C_{ps} (F)
Before cycles (Dark)	19.0	10.8	4.01	2.18	764μ
After 500 cycles (Dark)	19.6	5.10	5.46	3.63	2.69m
After 500cycles (Light)	17.8	4.11	9.54	10.1	293μ

Table 4. Values of parameters from the Nyquist plot in figure 20 using the equivalent circuit model in figure 11a

4. Conclusion

In this study, we reported a solar energy-assisted lithium-ion battery, which is combined with solar energy and a lithium-ion battery, unlike conventional solar-rechargeable battery. We tried to increase the capacitance of the battery by using the light absorption property of the active materials. We figured out the effects of light irradiation and change in the electrochemical properties by preparing WO_3 electrode as an anode under light compared to dark conditions. The capacitances and stability of the WO_3 electrode were increased under light irradiation due to the photogenerated electrons. The photogenerated electrons can be affected not only by the diffusion-controlled intercalation effect but also by the surface-controlled capacitance effect to increase the capacitance. The light effects are maximized under continuous light irradiation and further affect the extraction process than the intercalation process. Furthermore, we observed that the generated electrons by light irradiation can be accumulated. The accumulated photogenerated electron facilitates intercalation/extraction of lithium ions under light irradiation.

We provided new strategies for research for developing energy storage systems with thin, small, and light, and also meaningful information for the use of the sunlight. We expect the solar energy-assisted lithium-ion battery can be helpful to overcome the limitations of energy storage systems with physical characteristics such as

wearable devices, which are limited by physical size and thickness. However, we need continuously extensive effort because the capacitance and stability of the electrode for practical application are still low. To increase the capacitance, it is necessary to change the structure or material of the anode and study the cathode and electrolyte. In addition, it is required to develop a coating method for an efficient and stable electrode with a flexible substrate in order to be applied to a wearable device.

5. References

1 T. Kim *et al.* Applications of Voltammetry in Lithium Ion Battery Research. *Journal of Electrochemical Science and Technology* **11**, 14-25 (2020).

2 H. Kim *et al.* Exploring anomalous charge storage in anode materials for next-generation Li rechargeable batteries. *Chemical Reviews* **120**, 6934-6976 (2020).

3 J. Huang *et al.* Recent progress of rechargeable batteries using mild aqueous electrolytes. *Small Methods* **3**, 1800272 (2019).

4 Y. He *et al.* Atomistic conversion reaction mechanism of WO3 in secondary ion batteries of Li, Na, and Ca. *Angewandte Chemie* **128**, 6352-6355 (2016).

5 Q. Li *et al.* Solar energy storage in the rechargeable batteries. *Nano Today* **16**, 46-60 (2017).

6 M. M. Khan *et al.* Metal oxides as photocatalysts. *Journal of Saudi Chemical Society* **19**, 462-464 (2015).

7 S. Wang *et al.* Advances on tungsten oxide based photochromic materials: strategies to improve their photochromic properties. *Journal of Materials Chemistry C* **6**, 191-212 (2018).

8 J. Kim *et al.* Platinized WO_3 as an environmental photocatalyst that generates OH radicals under visible light. *Environmental Science & Technology* **44**, 6849-6854 (2010).

9 Y. Li *et al.* Preparation of oxygen-deficient WO_{3-x} nanosheets and their characterization as anode materials for high-performance Li-ion batteries. *Electrochimica Acta* **298**, 640-649 (2019).

10 P. R. Somani *et al.* Electrochromic materials and devices: present and future. *Materials chemistry and physics* **77**, 117-133 (2003).

11 P. Yang *et al.* Large scale fabrication of pseudocapacitive glass windows that combine electrochromism and energy storage. *Angewandte Chemie* **126**, 12129-12133 (2014).

12 J.-C. Chou *et al.* Electrochemical analysis of photoelectrochromic device combined dye-sensitized solar cell. *IEEE Transactions on Nanotechnology* **13**, 954-962 (2014).

13 C. An *et al.* Nanoporous Cu@Cu_2O hybrid arrays enable photo-assisted supercapacitor with enhanced capacities. *Journal of Materials Chemistry A* **7**, 15691-15697 (2019).

14 B. Tryba *et al.* Photocatalytic activity of TiO_2-WO_3 composites. *International Journal of Photoenergy* **2009**, 1-7 (2009).

15 I. M. Szilágyi *et al.* WO_3 photocatalysts: Influence of structure and composition. *Journal of catalysis* **294**, 119-127 (2012).

16 S. Pan *et al.* Wearable solar cells by stacking textile electrodes. *Angewandte Chemie* **126**, 6224-6228 (2014).

17 L. Hu *et al.* Thin, flexible secondary Li-ion paper batteries. *ACS nano* **4**, 5843-5848 (2010).

18 Z. Chen *et al.* A three dimensionally interconnected carbon nanotube–conducting polymer hydrogel network for high performance flexible battery electrodes. *Advanced Energy Materials* **4**, 1400207 (2014).

19 W. Zhao *et al.* High capacity WO_3 film as efficient charge collection electrode for solar rechargeable batteries. *Journal of Power Sources* **350**, 28-34 (2017).

20 D. Schmidt *et al.* Photo rechargeable electric energy storage systems. *Advanced Energy Materials* **6**, 1500369 (2016).

21 P. Liu *et al.* A solar rechargeable battery based on polymeric charge storage electrodes. *Electrochemistry communications* **16**, 69-72 (2012).

22 V. Subramanian *et al.* Nanocrystalline TiO_2 (anatase) for Li-ion batteries. *Journal of Power Sources* **159**, 186-192 (2006).

23 H. Liu *et al.* Graphitic carbon conformal coating of mesoporous TiO_2 hollow spheres for high-performance lithium ion battery anodes. *Journal of the American Chemical Society* **137**, 13161-13166 (2015).

24 J. Chen *et al.* α Fe_2O_3 nanotubes in gas sensor and lithium ion battery applications. *Advanced Materials* **17**, 582-586 (2005).

25 J. M. Jeong *et al.* Hierarchical hollow spheres of Fe_2O_3@Polyaniline for lithium ion battery anodes. *Advanced Materials* **25**, 6250-6255 (2013).

26 X.-Y. Xue *et al.* SnO_2/WO_3 core–shell nanorods and their high reversible capacity as lithium-ion battery anodes. *Nanotechnology* **22**, 395702 (2011).

27 M. S. Koo *et al.* In situ photoelectrochemical chloride activation using a WO_3 electrode for oxidative treatment with simultaneous H_2 evolution under visible light. *Environmental science & technology* **53**, 9926-9936 (2019).

28 J. Luo *et al.* Photoelectrochemical degradation of naphthol blue black diazo dye on WO_3 film electrode. *Electrochimica Acta* **46**, 2913-2922 (2001).

29 V. Barsykov *et al.* The influence of polymer binders on the performance of cathodes for lithium-ion batteries. *Materials Sciences and Applied Chemistry* **21**, 67-71 (2001).

30 K. Qi *et al.* In-situ transmission electron microscopy imaging of formation and evolution of Li_xWO_3 during lithiation of WO_3 nanowires. *Applied Physics Letters* **108**, 233103 (2016).

31 S. S. Kalanur *et al.* Facile growth of aligned WO_3 nanorods on FTO substrate for enhanced photoanodic water oxidation activity. *Journal of Materials Chemistry A* **1**, 3479-3488 (2013).

32 F. Liua *et al.* Ultrathin tungsten oxide nanowires: oleylamine assisted nonhydrolytic growth, oxygen vacancies and good photocatalytic properties. *Royal Society of Chemistry* **5**, 77423-77428 (2015).

33 Z. Jiao *et al.* Hydrothermally grown nanostructured WO_3 films and their electrochromic characteristics. *Journal of Physics D: Applied Physics* **43**, 285501 (2010).

34 G. Kim *et al.* Solar-rechargeable battery based on photoelectrochemical water oxidation: Solar water battery. *Scientific reports* **6**, 33400 (2016).

35 D. Wei *et al.* A nanostructured electrochromic supercapacitor. *Nano Letters* **12**, 1857-1862 (2012).

36 Z. Liu *et al.* Voltage issue of aqueous rechargeable metal-ion batteries. *Chemical Society Reviews* **49**, 180-232 (2020).

37 T. Zhu *et al.* Nanostructured tungsten trioxide thin films synthesized for photoelectrocatalytic water oxidation: a review. *ChemSusChem* **7**, 2974-2997 (2014).

38 E. Patrick *et al.* Corrosion of tungsten microelectrodes used in neural recording applications. *Journal of Neuroscience Methods* **198**, 158-171 (2011).

39 T. Brezesinski *et al.* Templated nanocrystal-based porous TiO_2 films for next-generation electrochemical capacitors. *Journal of the American Chemical Society* **131**, 1802-1809 (2009).

40 M. Meenakshi *et al.* Studies on electrochromic properties of RF sputtered vanadium oxide: tungsten oxide thin films. *Materials Today: Proceedings* **3**, 30-39 (2016).

41 J. Guo *et al.* Prominent electrochromism achieved using aluminum ion insertion/extraction in fmorphous WO_3 films. *The Journal of Physical Chemistry C* **122**, 19037-19043 (2018).

42 K. Zhang *et al.* Rational design and kinetics study of flexible sodium-ion full batteries based on binder-free composite film electrodes. *Journal of Materials Chemistry A* **7**, 9890-9902 (2019).

43 H. Lindström *et al.* Li^+ ion insertion in TiO_2 (anatase). 2. Voltammetry on nanoporous films. *The Journal of Physical Chemistry B* **101**, 7717-7722 (1997).

44 B. Das *et al.* Carbothermal synthesis, spectral and magnetic characterization and Li-cyclability of the Mo-cluster compounds, $LiYMo_3O_8$ and $Mn_2Mo_3O_8$. *Electrochimica Acta* **54**, 3360-3373 (2009).

45 C. T. Cherian *et al.* Morphologically robust $NiFe_2O_4$ nanofibers as high capacity Li-ion battery anode material. *ACS applied materials & interfaces* **5**, 9957-9963 (2013).

46 X. Fan *et al.* Porous thin-wall hollow Co_3O_4 spheres for supercapacitors with high rate capability. *Applied Sciences* **9**, 4672 (2019).

47 S. A. Abbas *et al.* Preparation of mesoporous microspheres of NiO with high surface area and analysis on their pseudocapacitive behavior. *Electrochimica Acta* **193**, 145-153 (2016).

48 J. Wang *et al.* Pseudocapacitive contributions to electrochemical energy storage in TiO_2 (anatase) nanoparticles. *The Journal of Physical Chemistry C* **111**, 14925-14931 (2007).

49 L. F. Que *et al.* Pseudocapacitance of TiO_{2-x}/CNT anodes for high performance quasi solid state Li ion and Na ion capacitors. *Small* **14**, 1704508 (2018).

50 Y. Jiang *et al.* Definitions of pseudocapacitive materials: a brief review. *Energy & Environmental Materials* **2**, 30-37 (2019).

51 T. Brezesinski *et al.* Ordered mesoporous α-MoO_3 with iso-oriented nanocrystalline walls for thin-film pseudocapacitors. *Nature materials* **9**, 146-151 (2010).

52 D. Chao *et al.* Array of nanosheets render ultrafast and high-capacity Na-ion storage by tunable pseudocapacitance. *Nature communications* **7**, 1-8 (2016).

53 H. Jiang *et al.* Hollow $LiMn_2O_4$ nanocones as superior cathode materials for Lithium ion batteries with enhanced power and cycle performances. *Small* **10**, 1096-1100 (2014).

Solar energy-assisted lithium-ion battery using photoelectrochromic property

Taeheui Kim

Department of Chemical Engineering, The Graduate School,
Pukyong National University

Abstract

As an alternative to overcome a limit on the capacity of thin-battery, we have tried integrating solar energy into the battery system and improving the electrochemical properties of batteries. We refer to this concept and design as a "solar energy-assisted lithium-ion battery". Tungsten oxide (WO_3) electrode was prepared as an anode of the solar energy-assisted lithium-ion battery, and its electrochemical properties under the sunlight irradiation were measured and analyzed. Furthermore, we examined sunlight irradiation effects during lithiation/delithation. When the light was irradiated to the WO_3 electrode, the capacitances were increased compared to that measured under the dark conditions. It is attributed to the photocatalytic property of WO_3 that can generate photoelectrons by light irradiation. The photoelectrons improve the capacities by participating in the intercalation of lithium ions and facilitating electrons transport. The effect of light is maximized under continuous light irradiation, and the capacitances were maintained under intermittent light irradiation. This results from the accumulation of photoelectrons by light irradiation. The wide working potential of WO_3 affects chemical stability under dark conditions. However, the stability of WO_3 was improved by light irradiation, which is attributed to the lithiation/delithiation with a narrow working potential of WO_3 due to the photogenerated electrons. We expect that this approach could provide an alternative solution to solve the battery problems which are limited by the device structure.